Measurement 222 (2023) 113640

Contents lists available at ScienceDirect

Measurement

journal homepage: www.elsevier.com/locate/measurement

Roughness evaluation of turned composite surfaces by analysis of the shape of autocorrelation function

Przemysław Podulka [a], Wojciech Macek [b,*], Beata Zima [b], Grzegorz Lesiuk [c], Ricardo Branco [d], Grzegorz Królczyk [e]

[a] Faculty of Mechanical Engineering and Aeronautics, Rzeszow University of Technology, Powstancow Warszawy 12, 35-959 Rzeszów, Poland
[b] Faculty of Mechanical Engineering and Ship Technology, Gdańsk University of Technology, Narutowicza 11/12, 80-233 Gdańsk, Poland
[c] Faculty of Mechanical Engineering, Wroclaw University of Science and Technology, Smoluchowskiego 25, 50-370 Wrocław, Poland
[d] Department of Mechanical Engineering, CEMMPRE, ARISE, University of Coimbra, 3030-788 Coimbra, Portugal
[e] Faculty of Mechanical Engineering, Opole University of Technology, 45-271 Opole, Mikolajczyka 5, Poland

ARTICLE INFO

Keywords:
Surface topography
Measurement
High-frequency measurement noise
Autocorrelation function
Autocorrelation function shape analysis

ABSTRACT

In this paper, the application of an Autocorrelation Function for the characterisation of surface topography was validated. The roughness evaluation of turned composite surfaces was supported by sophisticated studies of the Autocorrelation Function properties, considering especially the shape of the function. Details were measured with the optical method. The selection of the surface roughness evaluation procedures was carried out based on the Autocorrelation Function for both profile and areal analyses. Moreover, the application of various types of regular analysis methods, proposed in commercial software, like regular Gaussian regression and robust Gaussian functions, median de-noising, regular isotropic Spline, and fast Fourier transform filters, was proposed for the evaluation of surface topography parameters from the ISO 25178 standards. It was found that many common techniques, like commonly used filters, spectral analysis, and characterisation of texture direction, were supported by the proposed Autocorrelation Function studies. Moreover, the hard thresholding technique was found to be valuable in the comprehensive noise-suppression analysis.

1. Introduction

Variety in the application of surface topography analysis can indicate its growing significance in plenty of areas directly related to surface science. Much valuable information can be received straightly from surface texture studies. Rosenkranz et al. [1] imparted that precise surface texture analysis help to understand the possibilities of reducing friction or wear. Trzepiecinski et al. [2] related sheet deformation with a variation of the parameters of surface texture parameters and the value of friction coefficient. Harlin et al. [3], in general, affected the surface roughness on tribological performance in sliding contacts.

Staying with material properties, Deng et al. [4] linked multiaxial stresses with geometric discontinuities, like holes, and grooves, characterised when surface topography is studied. Furthermore, multiaxial fatigue was comprehensively studied by Branco et al. [5]. Rozumek et al. [6] presented the results of fatigue crack growth subjected to bending with structural considerations. Szala et al. [7], respectively, connected the surface texture parameters with cavitation erosion resistance as well. Generally, the functional properties of the surface were related by Abdel-Aal [8] with its roughness.All studies, reflected in various areas of surface topography studies, can be prone to numerous errors that may arise during the surface measurement, surface analysis, or comparison of its properties. Measurement errors and errors in data analysis preparation were often closely examined by Podulka [9] and Dzierwa et al. [10], respectively. These two actions are typically treated as a single operation, and the errors associated with both processes are generally classified as measurement errors.

Numerous types of errors can affect the characterisation of surface measurement results, especially for optical techniques. An example of this type of measurement is interferometry. De Groot in [11] introduced critically the surface topography interferometric measurement indicating its main disadvantages. A comprehensive presentation of all issues associated with optical measurements was presented by Leach in [12]. One frequently examined error is measurement noise [13]. Muhamedsalih et al. [14] classified its compensation as a challenging

* Corresponding author.
E-mail addresses: p.podulka@prz.edu.pl (P. Podulka), wojciech.macek@pg.edu.pl (W. Macek), beazima@pg.edu.pl (B. Zima), grzegorz.lesiuk@pwr.edu.pl (G. Lesiuk), ricardo.branco@dem.uc.pt (R. Branco), g.krolczyk@po.opole.pl (G. Królczyk).

https://doi.org/10.1016/j.measurement.2023.113640
Received 7 July 2023; Received in revised form 26 September 2023; Accepted 29 September 2023
Available online 30 September 2023

Nomenclature

ACF	autocorrelation function
D-ACF	double autocorrelation function analysis (double-ACF)
FFTF	fast Fourier transform filter
FT	Fourier transform
GRF	Gaussian regression filter
HFN	high-frequency noise
HFNS	high-frequency noise surface
L-surface	long-wavelength surface
LSPL	least square plane
MDF	median denoising filter
MQCL	minimum quantity cooling lubrication
NMPs	non-measured points
NS	noise surface
PSD	power spectral density
RGRF	robust Gaussian regression filter
RMS	root mean square
S-filter	filter removing small-scale components
S-L surface	surface received after S- and L- filtering
S-surface	small-wavelength surface
SF	regular isotropic spline filter
TD	texture direction
WLI	white light interferometry
Pt	total height of the profile, μm
Sa	arithmetic mean height, μm
Sal	auto-correlation length, mm
Sdq	root mean square gradient
Sdr	developed interfacial areal ratio, %
Sk	core roughness depth, μm
Sku	kurtosis
Smc	inverse areal material ratio, μm
Smr	areal material ratio, %
Sp	maximum peak height, μm
Spc	peak curvature, 1/mm
Spd	peak density, $1/mm^2$
Spk	reduced summit height, μm
Sq	root mean square height, μm
Ssk	skewness
Std	texture direction, °
Str	texture parameter
Sv	maximum valley depth, μm
Svk	reduced valley depth, μm
Sz	the maximum height of the surface, μm

task to be resolved. From the fundaments, according to the ISO standards [13] definition, measurement noise can be designated as the noise added to the output signal when the ordinary use of the measuring instrument occurs. A closely related ISO definition is instrument noise, which was supposed by Vanrusselt et al. [15] to be the lowest possible measurement noise value under ideal conditions.

The measurement noise was subjected by Leach et al. [16] to be analysed depending on its bandwidth. Considering the 'noise density' [17], one of the discussed topics is to reduce high-frequency measurement errors [18]. De Groot argued that high-frequency measurement noise can be caused by both mechanical instability and environmental factors [19]. However, considering most cases, high-frequency noise is generally caused by vibration [20].

When reviewing procedures for defining measurement noise, Gomez et al. [21] began by considering the effect of random noise on the final topography map. This can occur when using Coherence Scanning Interferometry (CSI) and averaging a sequence of repeated surface topography measurements, comprehensively studied by Giusca et al. in [22]. In contrast to the averaging methods, the measurement noise, in the selected bandwidth, such as in the high-frequency domain, can be evaluated when characterising the results received after digital filtering, e.g. comparing the spline techniques [23]. Furthermore, the advantages of the application of areal and profile studies of surface topography parameters were illustrated by Macek et al. in [24]. Results obtained when measurement noise is suppressed can be defined as the Noise Surface (NS), which should possess some necessary properties. All of those characteristics, such as dominant frequency or not containing non-noise components (features) were thoroughly examined by Podulka [25].

Functions directly related to frequency characterisation are crucial in the definition of high-frequency measurement noise. Spectral analysis is a popular approach, with the power spectral density (PSD), or power spectrum, being a representative example. Reina et al. [26] used the PSD for improving the estimator to evaluate terrain online during normal operations of driving assistance systems. Krolczyk et al. [27] applied the PSD for comparing surfaces after dry and MQCL turning processes. Consequently, Kalisz et al. [28] compared the effects of various machining methods (milling-burnishing, milling and polishing) with the usage of PSD characteristics. Nieslony et al. [29] found PSD allows analysis of the drilling process in different layers of clad materials as well.

The PSD of a surface, which represents a mathematical tool, decomposes the surface into contributions from different spatial frequencies (wave vectors). Simplifying, it provides a way of representing the distribution of signal frequency components. Mathematically, the PSD is the Fourier transform (FT) of the Autocorrelation Function (ACF) of the signal, which contains only the power and not the phase. Leach et al. [30] searching for the limitations, found that the PSD cannot be used to characterize all components of the surface error. Moreover, unlike the PSD, the ACF was noted by Whitehouse [31] as more useful for the characterisation of random surfaces. However, both functions were presented by Michalski [32] as useful and not mutually exclusive.

The PSD curve can be divided into three regions: low-frequency region, intermediate frequency region, and high-frequency region. Each of the regions can play a significant role in the characterisation of surface roughness. The first two regions play a significant role in characterizing the surface roughness. The first two regions are associated with the overlap of craters and the mechanism for removing indentations cutting edges, respectively. In constrast, the high-frequency region is linked to the removal of micro-dents [33]. The PSD was primarily introduced as an effective tool for characterizing the surface profiles, enabling the extraction of both vertical and lateral information. It provides insights into the influence of roughness at different spatial frequency regions on the overall roughness, a dimension that cannot be determined using arithmetic average or root mean square roughness [34].

Generally, using statistical functional parameters can be an effective way to extract surface topography features. The ACF of the roughness profile can reveal random and periodic features that may be present in the generated surface. Furthermore, the relative contribution of the electrolytic dissolution and the pure mechanical grinding in electrochemical grinding (ECG) can also be received from the ACF analysis, as introduced by Roy et al. in [35]. It has been found by Wang et al. [36] that the apparent isotropy and aperiodicity of belt surfaces are confirmed by examining the shape of the ACF, especially its symmetry. In general, the anisotropy of all machined surfaces can be exhaustively examined by analysing the ACF properties [37].

It has been found by Podulka [38] and Hreha et al. [39] that the overall assessment of the ACF can be particularly significant in the feature-based or frequency-based studies of machined surfaces, correspondingly. It was also assumed in [40] that sizes, densities and

distributions of features can significantly influence the data processing methods as well. The edge effect, also known as the end effect, can be also reduced when comprehensive studies of some general functions are provided, especially for areal form removal [41] (ISO definition of the L-surface [42]) processes [43]. Extensive investigation of the ACF is relevant in defining certain types of measurement noise, particularly those in specific frequency domains [44]. In previous studies from the authors, some differences were observed especially for the centre part of the function, where the maximum value was obtained. The occurrence of high-frequency components was noticeable when the ACF value increased more rapidly. This property was found to be suitable for selected types of topographies.

Moreover, the accuracy of the ACF noise detection was influenced by the direction of the profile characterisation (extraction). Previous research papers have demonstrated that the direction of profile extraction plays a crucial role in improving accuracy during the high-frequency noise identification and reduction process [25]. Among the suggested extraction orientations - horizontal, vertical, and oblique – special attention has been given to the oblique direction. In this case, it is selected according to the direction of the machining trace, often called as the treatment trace profile, leading to improved detection accuracy for high-frequency measurement noise. In cases involving surfaces with deterministic patterns, the application of profile characterisation alongside areal data is justified. Thus, simultaneous analysis of both areal and profile data is essential in such cases.

Consequently, the high-frequency noise was not suitably studied for the turned details, especially for those made of composite material. Finding the dependence between the noise occurrence and ACF properties can be valued according to the function availability. Finally, reducing the measurement noise can be essential to reduce errors in the calculation of surface texture parameters. Thus, the main purpose of this paper is to provide an appropriate response from the ACF characterisation to the process of defining high-frequency measurement errors.

2. Materials and methods

2.1. Analysed surfaces

The turned composite surfaces were measured, studied, and characterized using the ACF technique. Generally, machining composite materials are difficult due to their anisotropic and non-homogeneous structure. Moreover, the high abrasiveness of their reinforcing constituents is a serious limitation as well, as mentioned by Teti et al. [45]. However, turning, classified as a conventional machining process, can be applied to composite materials. Fig. 1 presents representative examples of the surface topography of machined composites.

Various cross-hatch angles of composite surface machining were studied varying from 30° to 60°. The cutting speed was 50 m/min, the feed rate was 0.1 mm/rev, and the depth of cut was 0.25 mm.

Fig. 2 includes examples of analysed surface topographies considering both contour map plots (a) and isometric views (b). Moreover, the selected ISO 25178 standard parameters (c) were presented with areal (d) and profile (e) ACFs. In addition, subfigures (e) and (f) show the PSD and TD graphs, respectively. The ISO 25178 texture parameters were also analysed.

2.2. Measurement process

All of the analysed surfaces were measured with the non-contact measurement device, the white light interferometer (WLI [46]) Talysurf CCI Lite. It was equipped with the following: a height resolution equal to 0.01 nm; and a measured area defined with 3.35 by 3.35 mm^2, including 1024 × 1024 measured points, respectively. The spacing was designated as 3.27 μm. Furthermore, a Nikon (5×/0.13 TI) objective was employed. More than 10 samples were measured for each type of surface cross-hatch angle (30°, 40°, 45°, and 60°).

For the analyses of the results obtained, areal digital filters processed with the TalyMap Gold (Digital Surf) software were used to obtain the ISO 25178 surface texture parameters, as follows: regular Gaussian regression filter (GRF), robust Gaussian regression filter (RGRF), regular isotropic spline filter (SF), median de-noising filter (MDF), and fast Fourier transform filter (FFTF).

Consequently, all of the applied data processing functions (i.e. power spectral density (PSD) calculated with the 'all directions method', autocorrelation function (ACF), and texture direction (TD)) were received and validated by using this source. The mathematical background of ACF and PSD methods can be found in reference [42]. The hard thresholding technique was also investigated with this source.

2.3. Applied methods

2.3.1. Proposed procedure for data pre-processing and errors compensation

The proposed procedure was initiated by filling the non-measured points (NMPs). The NMPs point heights were calculated by the smoothed shape from the neighbours' method proposed by the commercial software. Secondly, the outliers' existence was studied and hard thresholding was applied. The thresholding value varied in the range of 0.13 % – 99.87 %. Next, the third pre-processing proposed the levelling of the received measured data by the least-square plane (LSPL) technique for the horizontal positioning of the surface data.

In further steps, the received surface topography data were studied for the possible occurrence of high-frequency measurement noise. In this case, comprehensive studies of the shape of the ACF were proposed for the detection process improvements. It was found that the shape of ACF was modified in the maximum value (usually around the '1') when the high-frequency components were received in the measured topography

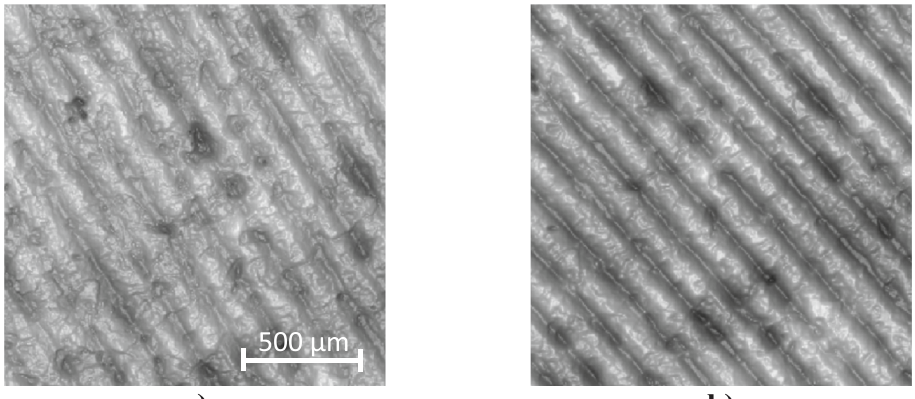

Fig. 1. Surface topography images of turned composites with machining cross-hatch angles approximately equal to (a) 30° and (b) 40°.

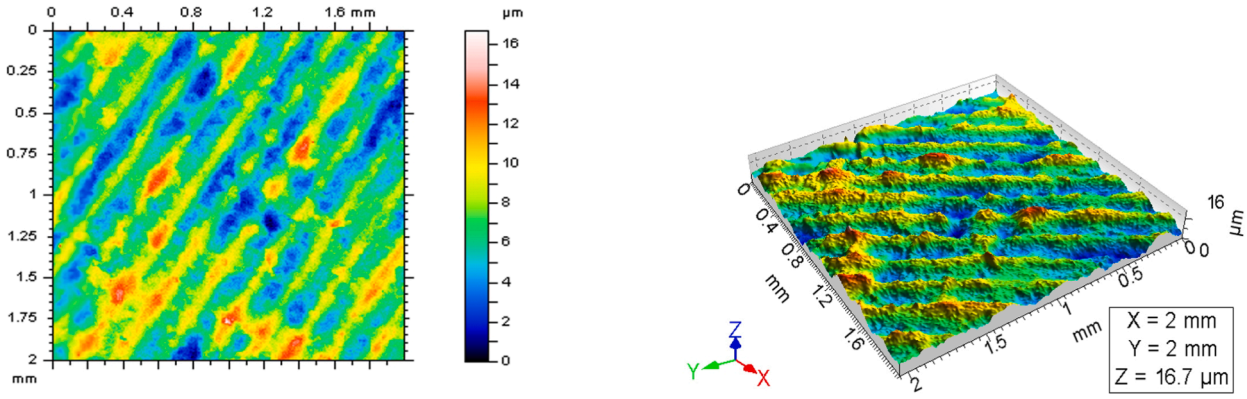

a) **b)**

Sq = 2.17 µm, *Ssk* = 0.178, *Sku* = 2.91, *Sp* = 9.91 µm, *Sv* = 6.81 µm, *Sz* = 16.7 µm, *Sa* = 1.73 µm,
Smr = 0.00221 %, *Smc* = 7.09 µm, *Sal* = 0.0645 mm, *Str* = 0.115, *Std* = 57.2 °,
Sdq = 0.113, *Sdr* = 0.637 = %, *Spd* = 45.5 1/mm^2, *Spc* = 0.0375 1/mm,
Sk = 5.2 µm, *Spk* = 2.05 µm, *Svk* = 1.05 µm

c)

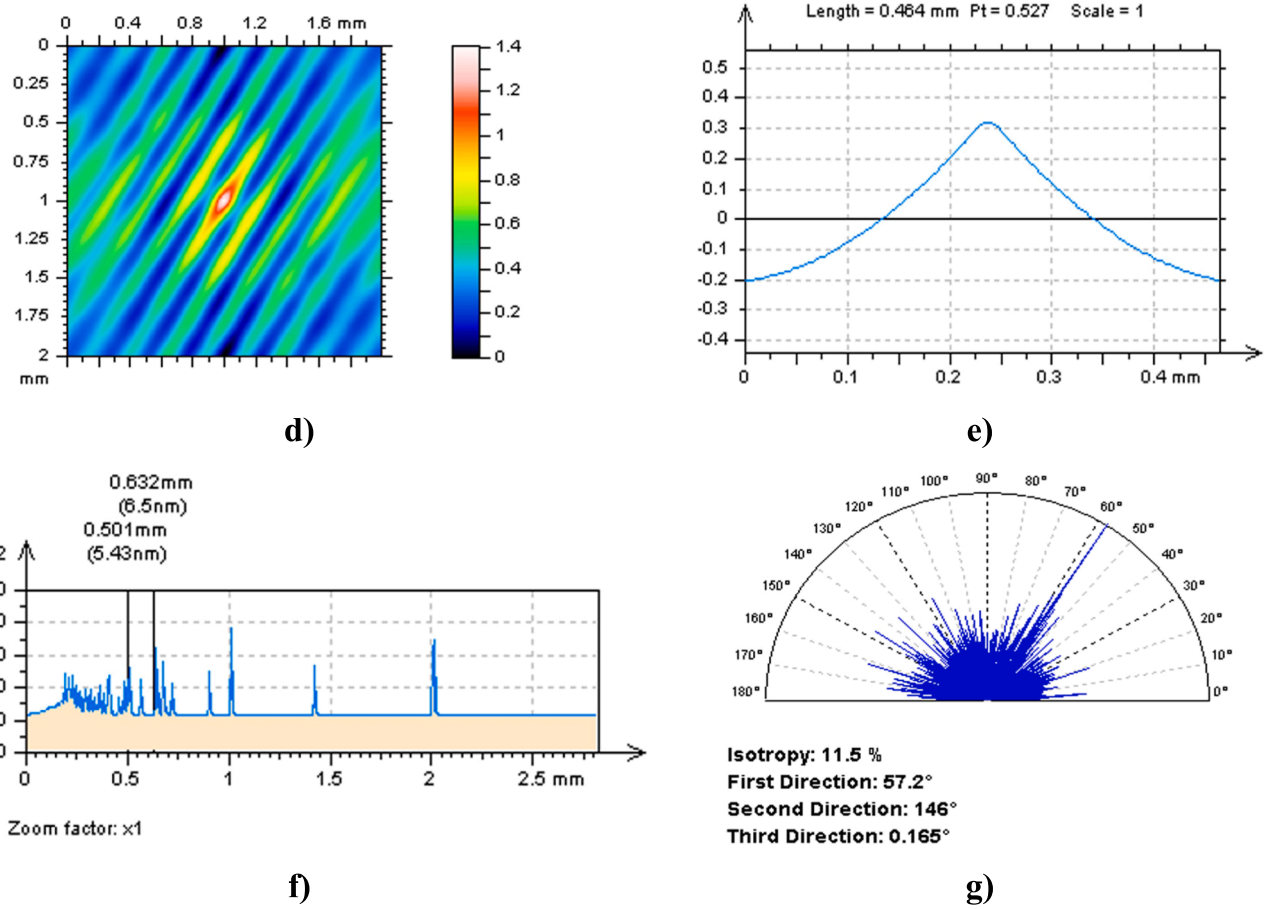

d) **e)** **f)** **g)**

Fig. 2. Contour map plots (a), isometric view (b), selected ISO 25178 texture parameters (c), the areal (d) and profile (e) ACFs, PSD (f) and TD graph (g) of a turned composite surface.

data [23]. Otherwise, the presence of high-frequency errors can be validated when the noisy data (noise surface) is studied. Proper noise surface properties are required [25].

The measurement noise can be reduced by repeating the measurement process. Nevertheless, for machined surfaces, where roughness control is usually required with in-line accomplishments, the time to reduce measurement errors and computing errors is crucial. As an alternative to the statistical noise compensation methods, digital filtering can be adopted. In this approach, the fast implementation of the filter algorithms is its biggest advantage. A common and frequently encountered issue is the selection of the appropriate filter and its bandwidth. If the cut-off value is chosen incorrectly, it can lead to a

significant increase in errors during the calculation of ISO 25178 texture parameters. Consequently, this can result in an accurate estimation of surface properties and misclassification of properly manufactured parts, including defects and rejected items. To minimise this problem, a comprehensive procedure for high-frequency measurement noise suppression is proposed in this paper, as presented in Fig. 3.

The filter and its bandwidth are studied to address noisy data that may contain proper frequencies. It is assumed that the data removed from the surface should contain the frequencies of the noise suppressed. In the specific case being studied, the noise surface (NS) is expected to consist of high-frequency components. The validation of the filter and its cut-off selection is proposed through a comprehensive analysis of the autocorrelation function (ACF) and power spectral density (PSD) of data functions, as well as thresholded ACF and PSD of the data, and the requirements for isotropic direction based on TD graph studies. Some improvements in the validation of the noise removal process were also achieved when studying profile data instead of areal data. However, it is important to note that the proposed characterization of noise profiles is influenced by the direction in which the profile is extracted and must be carefully specified.

Finally, a suitable filter and its bandwidth can be proposed to minimize errors in the calculation of ISO 25178 texture parameters from machined composite surface topographies.

2.3.2. *Reduction of errors in texture parameter calculation with an ACF shape and directional methods*

In previous studies of the ACF validation in the process of general surface topography analysis, Mattia et al. [47] indicated that using

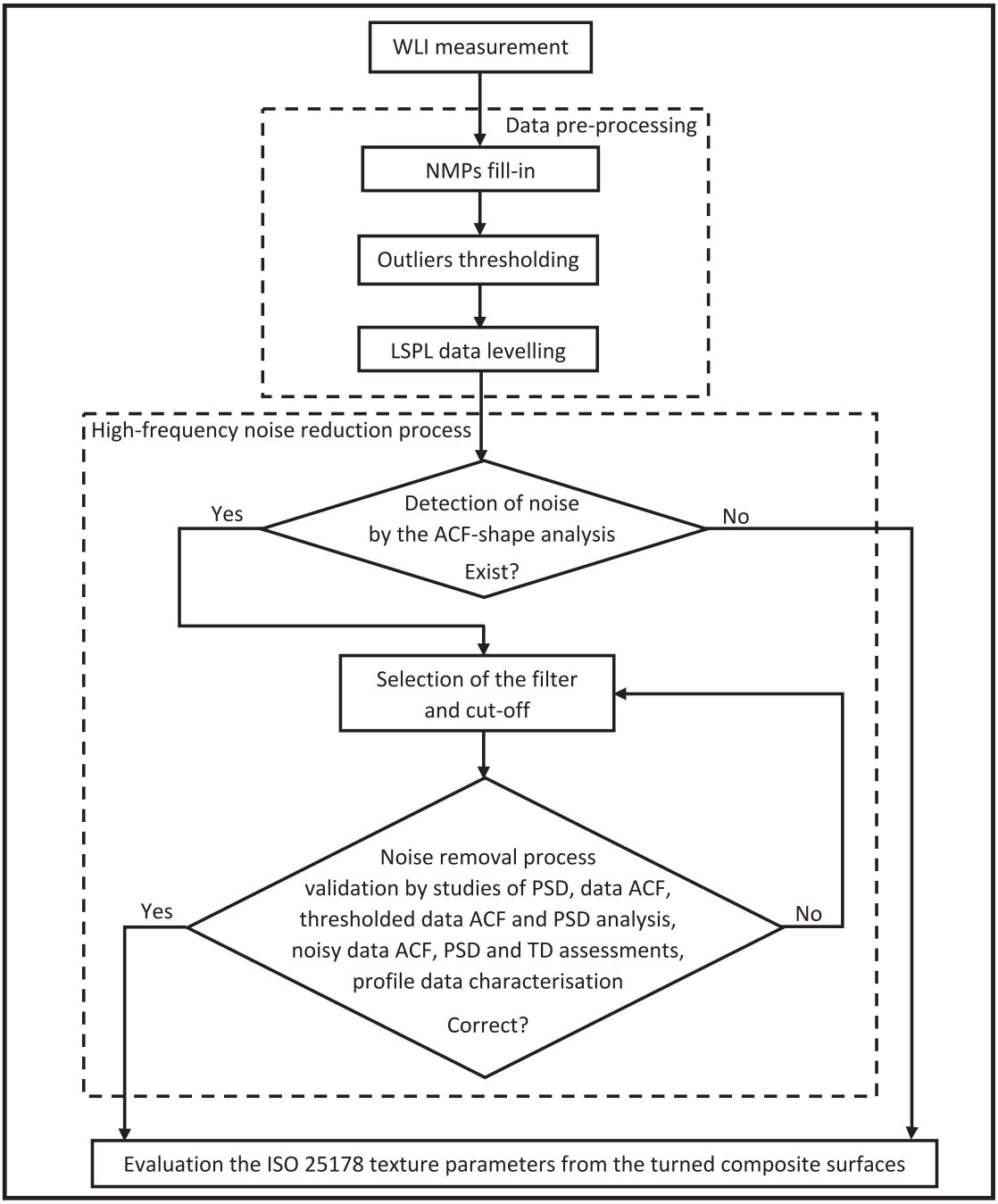

Fig. 3. The flow chart of the applied procedure.

simulated data, the shape of the ACF is sensitive to measurement resolution. Consequently, both the accuracy when the correlation length parameter is evaluated and its precision rely largely on the total extension of the measurements, studied by Oh et al. [48].

The shape of ACF can be particularly advantageous when measuring very long profiles. Thus, as found by Manninen et al. [49], the final data may need to be compiled from several bendwise ACFs to meet the experiment requirements. Additionally, research has shown that for very smooth surfaces, particularly those exhibiting fractal processes and, as concluded by Zhixiong et al. [50], the relative amplitude of the single-scale process determines the overall shape of the ACF. It was also found that the shape of the ACF can indicate the state of the surface [51].

The shape of ACF has also been examined by Podulka [23] in cases where high-frequency measurement errors need to be detected. It has been found that data containing noise data, included in the high-frequency domain, display a more rapid increase in ACF within the maximum value bandwidth compared to data with no content of those frequencies. Generally, the shape tends to modify from convex to concave near the '1′ value, as concluded in [23].

However, the process of detection of noise data, based on the analysis of the ACF shape, produces more direct results when examining profile data rather than areal data. This dependence was substantially enhanced for the detection (definition) of high-frequency noise. Some examples of modifications to the maximum value of the ACF (indicated by the marker in the e and f subfigures) are presented in Fig. 4. The ACF-shape method can be especially valuable when differences in the PSD functions are not observed (subfigures c and d) but noise data can be detected by analysing the associated profiles (subfigures a and b). Loew et al. [52] proved that the ACF-shape analysis technique can be highly satisfactory regardless of the size of the analysed detail.

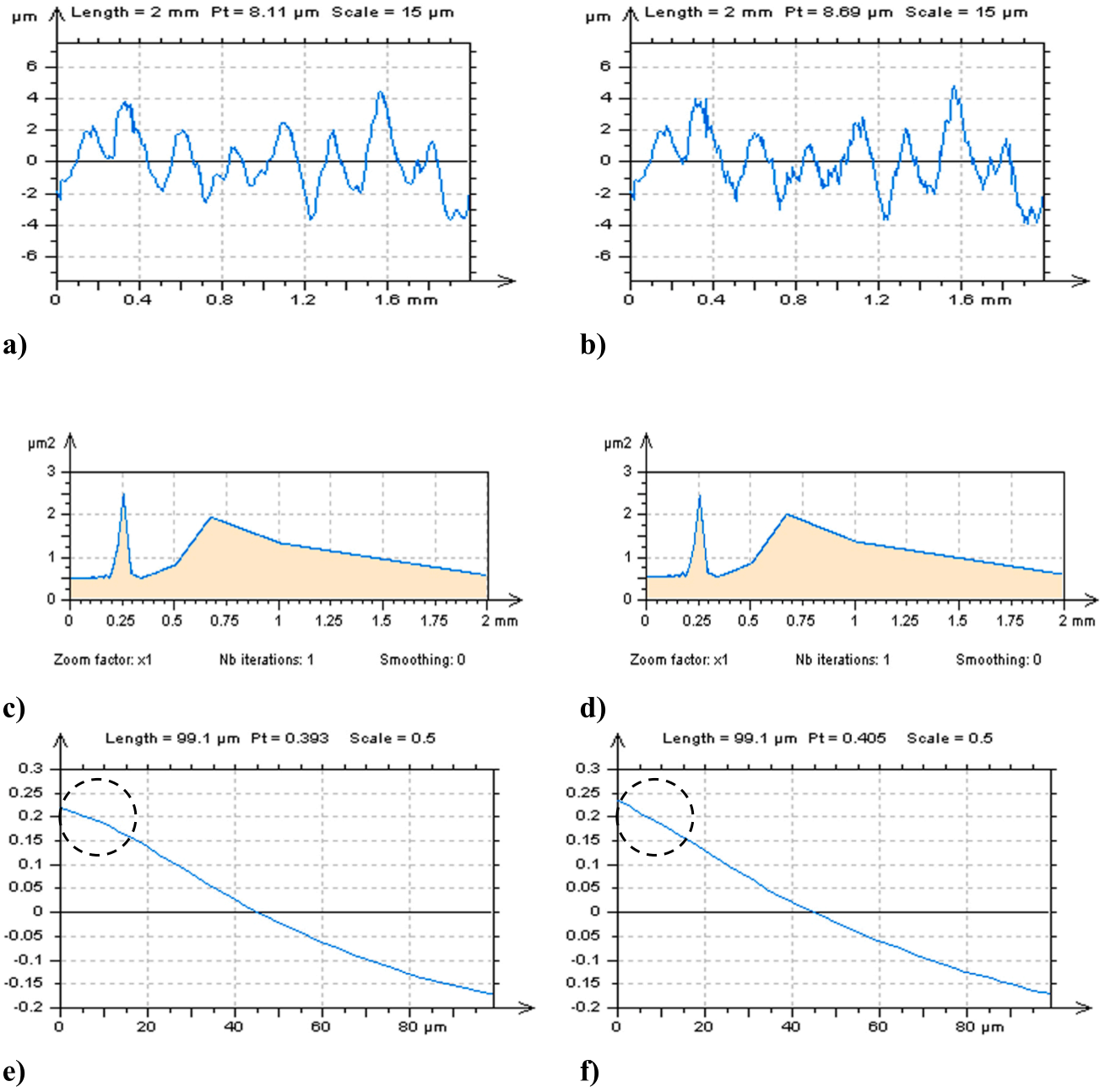

Fig. 4. Selected profiles (a,b), their PSDs (c,d) and ACFs (e,f), received from a turned composite surface for raw measured data (left column) and with generated high-frequency noise (right column).

Additionally to the ACF-shape method, the precision of detection of measurement noise in the high-frequency domain can be influenced by the direction of profile data extraction from an areal data [18]. Except for some horizontal and vertical directions, proceeding with the oblique (diagonal) directions, the treatment-trace direction was suggested. Previous studies have shown relying on the location of summits ('top') and valleys ('bottom') using the treatment-trace profile approach is effective in detecting high-frequency noise [40]. However, this scheme has been comprehensively studied only for specific types of surface topographies, such as turned surfaces (e.g. piston skirts, comprehensively studied by Shaw et al. in [53]) or laser-textured surfaces (e.g. titanium, presented by Convert et al. in [54]).

The combination of both ACF-shape and direction techniques can be highly advantageous in many surface-topography studies. Nevertheless, the type of machining may not give similar responses when the processed material varies. Fig. 5 presents the ACFs calculated for profiles extracted in various directions, including horizontal (a,b), vertical (c,d), diagonal (oblique) (e,f), and treatment-trace (g,h), as previously mentioned. It can be observed that differences either did not exist or were negligible in the investigated cases and, therefore, may not be relevant in the detection of high-frequency measurement noise occurrence. Furthermore, reducing noise with a selection of the cut-off value [25] is not achievable due to the lack of NS analysis. This characterisation requires additional methods to validate the occurrence of high-frequency measurement noise.

2.3.3. Improving ACF techniques with thresholding methods for a high-frequency measurement noise suppression

Lacks definition in high-frequency measurement noise, received through ACF-shape and direction methods, can be reduced by hard thresholding the raw measured data, as presented by Martha et al. in [55]. The thresholding technique can be applied to the measured data or, as proposed in the presented studies, can be applied to perform a more comprehensive characterisation of the surface roughness analysis functions. Fig. 7 shows some examples of the selection of the thresholding value (A1 and A2) based on the Abbott-Firestone curve (c,e).

Fig. 8 shows the application of the thresholding method to the ACF for improving the high-frequency noise reduction process. The differences in the NS contour map plot, indicating the noise occurrence, can be difficult to precisely determined (a,b), including its PSD (c,d) and ACF (e,f) characterisation. Some marked variations were only received when the ACF was thresholded (g,h). The received ACF could be classified as isotropic and with a dominant direction. Additionally, the procedure for defining the thresholding value was thoroughly examined, justified, and originally proposed in previous items [25,56].

The thresholded ACF can be used for both raw measured and thresholded data. In Fig. 9, the thresholded NSs were analysed for raw measurements and contained high-frequency noise surface topographies. Compared to non-thresholded data presented in the previous figure, some differences were detected with contour map plots (a,b) but, differences in PSD (c,d) characterisation were negligible. Further thresholding of the ACF data (e,f) may allow for a clear disparity. From the analysis of contour map plots of thresholded ACF data, some features not located in the required (high) frequency were identified (areas marked by the arrows in Fig. 9e).

Considering the necessary properties of NS, their thresholded data, and calculated PSD and ACF functions, it is not clear how they respond to the definition of high-frequency errors. However, the effectiveness of the thresholding technique on the ACF data is well-justified, and the technique can be considered promising with double thresholding, which includes limitations of raw measured data and ACF data obtained from those data. The double thresholding method starts with the thresholding of the noise-filtered data, e.g. by FFTF filtration, see Fig. 9a and 9b. Then, the ACF calculated from the received data is further thresholded, see Fig. 9e and 9f. This technique plays a crucial role in characterizing the required properties of properly defined noisy data (noise surface). The flow chart illustrating the double thresholding approach can be found in Fig. 6.

Additionally, direction studies (g,h) can provide insights into noise identification. The texture direction (TD) graph can be especially important in determining if the surface data are isotropic or not. In this study, it was found that analyzing the TD of thresholded ACF data has the potential to be profitable for identifying high-frequency errors.

2.3.4. Proposal of a profile analysis for filter cut-off selection improvements

Since material contact is studied as an areal performance [57], analysing surface topography with areal measurement and ISO texture parameters is completely justified and required in the process of surface tribological performance, like presented by Singh et al. in [58]. However, studies of profile data, investigated by Li et al. [59], can be essential and more advantageous than areal measurements, especially when studying contact mechanics and related damage issues. Some examples of profile data studies against areal measurements were noticeably improved in previous studies [23].

In addition, the profile characteristic can be more valuable in resolving many surface metrology problems, like edge-effect reduction and characterisation of anisotropic surface structures of additively-manufactured products, resolved by Zakharov et al. in [60] and [61], respectively. However, Ramulu et al. [62] found that profile characterisation can rely on the direction of the measurement, extraction, and accuracy of the data processes. Peta et al. [63] emphasized that, generally, surface roughness analysis requires mindful users or, at least, those who are properly guided.

Profile characteristics are useful for resolving some surface metrology issues, and much relevant information can be obtained from profile data extraction, like adhesion and corrosion creep, presented by Croll et al. [64], roughness prediction of milled surfaces, mentioned by El-Sonbaty et al. [65] or, more widely, wettability, indicated by Kubiak et al. in [66], superhydrophobicity, found by Yang et al. in [67], the roughness of a sanded wood surface, introduced by Hendarto in [68] and in the generation of data, experimental and simulation analyses on periodic roughness, completed by Carmignato et al. in [69].

When characterising the profile data, there are significant advantages to studying the profile view. Fig. 10 presents profiles obtained from a turned composite surface for both the raw measured (a) and data with simulated high-frequency noise (b). Except for the noise visibility, the total height of the profile (Pt) increased for the noise data compared to the measured data. When considering the ACF and its shape (c,d), especially in the central part of the function, differences did not exist or were negligible. The amplitude of the noise received after an FFTF (bandwidth 20 μm) filtering (e,f) was larger for the noised data than that in the measured data, at 1.2 μm and 0.676 μm, respectively. Moreover, the increase in noise amplitude was detectable with PSD characterisation (g,h), where the magnitude of high-frequency components was larger for the NS profile obtained from noisy data than that obtained from raw measured data.

In Fig. 11, the thresholding method is presented for the turned composite surface profile data. Previous studies have shown that spectrum (frequency) analysis can be more valuable for profile data than for an areal [9]. For profile characterisation, the ACF (a,b) was thresholded (c,d). The application of this technique was crucial in the detection of non-noise features from the NS profiles. The non-noise feature disclosure can be markedly improved for both profile views (c,d) and PSD (e,f) studies. The PSD, which represents the distribution of heights (pits), studied by Kanafi et al. [70], can provide information on dominant frequencies, considered by Ostasevicius et al. [71]. Reflecting the properly filtered NSs, or NS profiles, should contain only the analysed noise frequencies. In the presented studies, high-frequency components are expected to be present. The PSD of thresholded ACF data, filtered from those raw measured data contained a dominant frequency with a 0.101 mm bandwidth (g). The PSD calculated for thresholded ACF from the NS profile obtained from noisy data contained more dominant

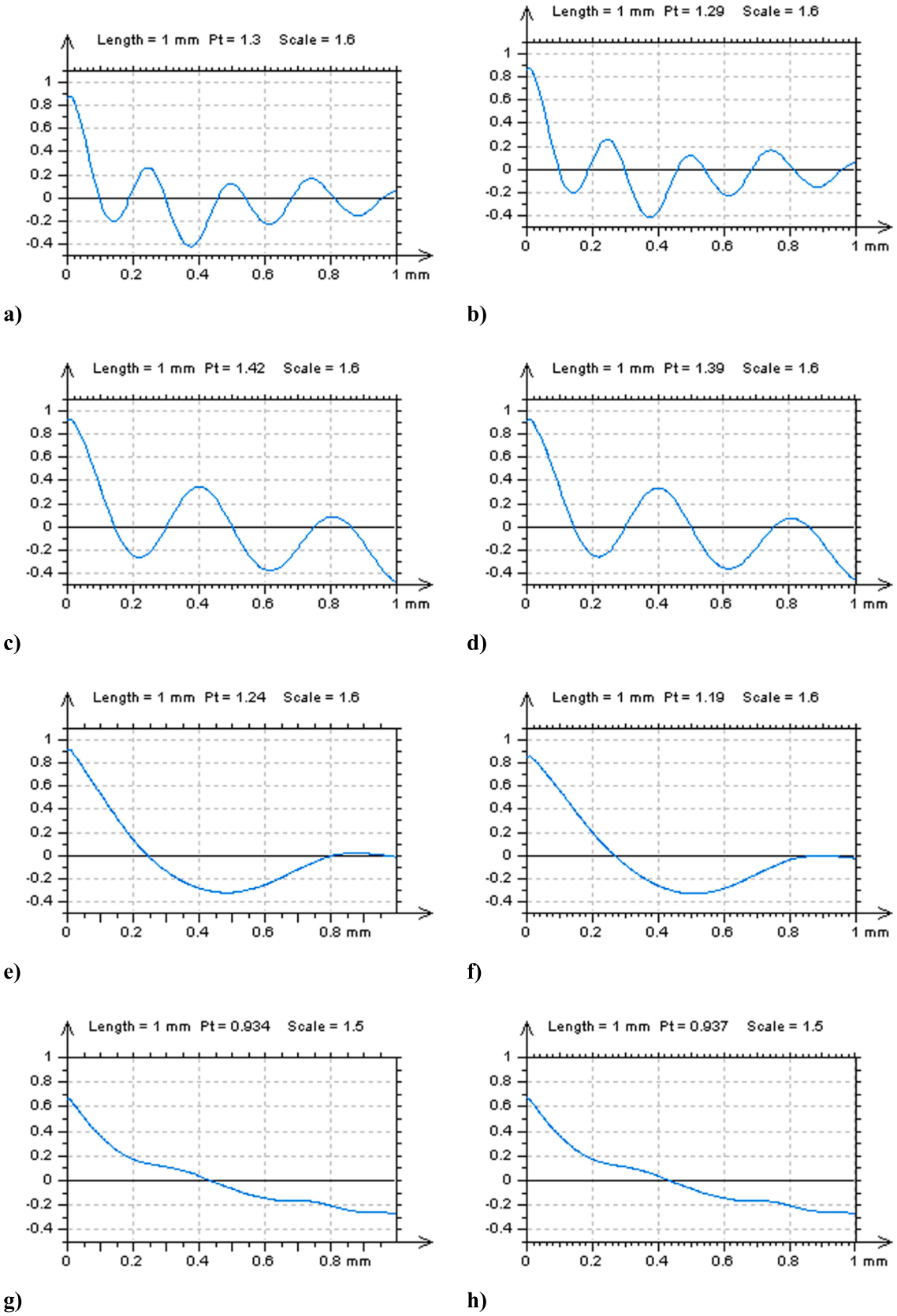

Fig. 5. Profiles extracted from an ACF with horizontal (a,b), vertical (c,d), diagonal (oblique) (e,f), and treatment-trace (g,h) directions, received from the raw measured surface (left column) and with generated high-frequency noise (right column).

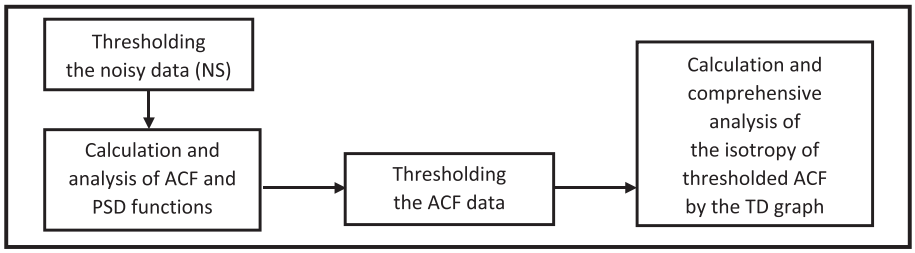

Fig. 6. The flow chart of the double thresholding method.

components located in the high-frequency domain (h).

Additional analysis can be performed when ACF is determined for the thresholded ACF data (g,h). This technique, shortly named double-ACF analysis (D-ACF), can be beneficial in the detection of non-noise components in NSs or NS profiles. The density of the dominant frequency component in the NS profile is equal to 0.10 mm, as shown in Fig. 10g. For non-noise data, a filter with a bandwidth equal to 3 times the measurement spacing was applied, which caused non-noise features to appear on the NS profiles. Improvements were observed in the NS profile containing high-frequency noise (Fig. 10*h*). Consequently, the D-ACF method can be valuable in detecting high-frequency noise in turned composite surface measurements.

3. Results and discussions

3.1. Definition of HFN by characterisation of the ACF

One of the major issues in surface metrology, as indicated by Chen et al. in [72], when analysing surface roughness is the definition of measurement errors. If statistical methods are included, it is difficult to separate the real data from those classified as errors. To address this problem, Kuo et al. [73] measured the same area repeatedly and provided a reasonable solution for assessing measurement repeatability. Nevertheless, data removed from that raw measurement can include some real results. Simultaneously, the reduction of measurement noise can be studied on the results of the data removed. Those data were previously defined as noise surfaces [25]. Considering the frequency of the suppressed noise data, the NS consisting of errors in the high-frequency domain was defined as high-frequency noise surface (HFNS) [9,18,23]. Generally, the properties [9] of NS (HFNS) can be found if the data are appropriately removed. Removing non-noise data from those raw measurements can increase errors in ISO 25178 parameters calculation and, correspondingly, lead to the misclassification of properly made parts as defective, as presented by Grabon et al. in [74]. Moreover, the methods for suppression of high-frequency measurement noise can be validated when the properties of NS are found.

Fig. 12 shows two different NSs obtained by filtering raw data from turned composite surfaces using Gaussian radial basis functions (GRF), subfigures (a,c,e,g), and spline functions (SF), subfigures (b,d,f,h). The cut-off was selected and compared between the two applied filtering methods according to recent standards [75], often referred to as the nesting index, e.g. by Li et al. [76]. Considering the studies of contour map plots of NSs, the ones calculated by the GRF contained features with one specified direction, indicated by arrows in Fig. 12a. A similar property was not observed in the NSs calculated by SF filtration in Fig. 12b. The directionality of the NSs indicates that the removed data contains non-noise features which are not desired.

Consequently, the filtration method responsible for non-noise feature occurrence on the removed data cannot be classified as suitable for the high-frequency measurement noise definition. Improving the above assumption can be considerably taken with the application of the thresholding technique. The thresholded ACF of the areal data can reduce the errors in an accurate definition of NS. The GRF method was found to be less effective for the reduction of high-frequency errors (Fig. 12c) compared to the SF filtration (Fig. 12d). Moreover, the PSD analysis revealed the dominant frequencies. The dominant frequency for the GRF was approximately, 0.2 mm. This distance is related to the distance between turning traces. In contrast, the dominant frequency for SF was in the high-frequency domain, indicating that the NS created by the SF method was isotropic, while the NS obtained by GRF was not (Fig. 12g and Fig. 12h).

However, both PSD and TD characterisations may not be unequivocal in certain cases. In Fig. 13, the NS calculated after the application of the median deviation filter (MDF) method, with a cut-off equal to 0.20 mm, is presented with its functions (PSD, TD, and ACF). When analysing the contour map plots of NS (a), no non-noise features were identified. PSD (b) and TD (c) seemed to confirm this finding. Notwithstanding, the throughout analysis of the ACF revealed the shortcomings of those techniques. Firstly, some non-noise (with specified direction) features were found on the ACF diagram (d). Secondly, the contour map plot of the thresholded ACF graph conferred the non-noise features (e). Additionally, the PSD of the thresholded ACF determined a dominant frequency similar to the distance between treatment traces (0.2 mm). Finally, TD and D-ACF analyses confirmed the non-isotropic properties of NS. All of these characteristics excluded the NS obtained by using the MDF technique from being potentially suitable for the reduction of high-frequency errors in surface roughness measurements. In this case, the ACF function, including the thresholding of the data, had to be reapplied.

3.2. Improving proposed methods in the filter cut-off selection

Selection of the cut-off value, often referred to as bandwidth, is a critical process that, when not validated appropriately, can cause enormous errors in the calculation of ISO 25178 surface texture parameters. Surface properties can be evaluated erroneously when the cut-off value is not determined properly. Historically, the cut-off was thought to generate a large number of errors in defining the long-frequency components (shape and waviness) of the surface. Many recent metrological problems have been identified around this issue as well [41]. However, when the surface roughness is evaluated, the S-L surface must be defined. The S-L surface analysis can be divided into two studies: firstly, areal form removal (definition of the L–surface); and, secondly, reduction of the high-frequency errors (designation of the S-surface). When the cut-off is properly selected for the shape and waviness (form) removal, the relevant bandwidth must be proposed for the reduction of high-frequency errors (noise).

In Fig. 14, the comprehensive analysis of the profiles extracted from various NSs, created by FFTF filtration with different cut-off values (0.10 mm, 0.20 mm and 0.30 mm) is presented. The first observation is related to the different amplitudes of the noise profiles (a). The greater the bandwidth selected, the larger the amplitude received. However, the amplitude cannot be a criterion for the noise separation method preference. The application of NS profile PSDs (b) and ACFs (c) may not adequately respond to these issues as well. Some more useful responses can be obtained by studying the central part of the ACF (d). It was found that both the data containing the high-frequency components and high-frequency data have their ACF increasing more rapidly than regular non-

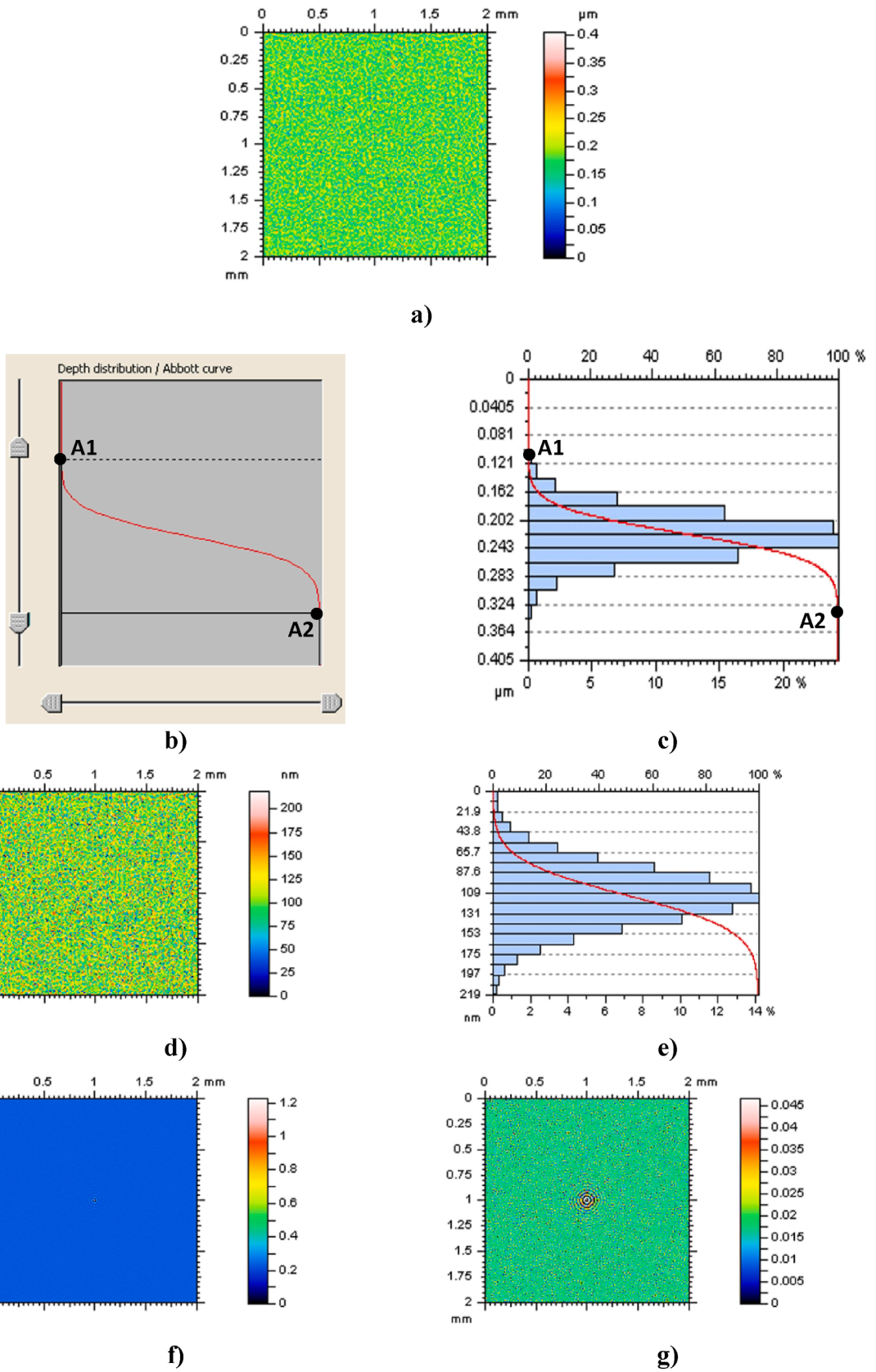

Fig. 7. The NS (a) obtained by FFTF (cut-off = 0.010 mm) filtering, the method of selection of the thresholding value (b) with the Abbott-Firestone curve (c), the thresholded NS (d) and its Abbott-Firestone curve (e), the ACF of thresholded NS (f) and the thresholded ACF of the thresholded noisy data (g).

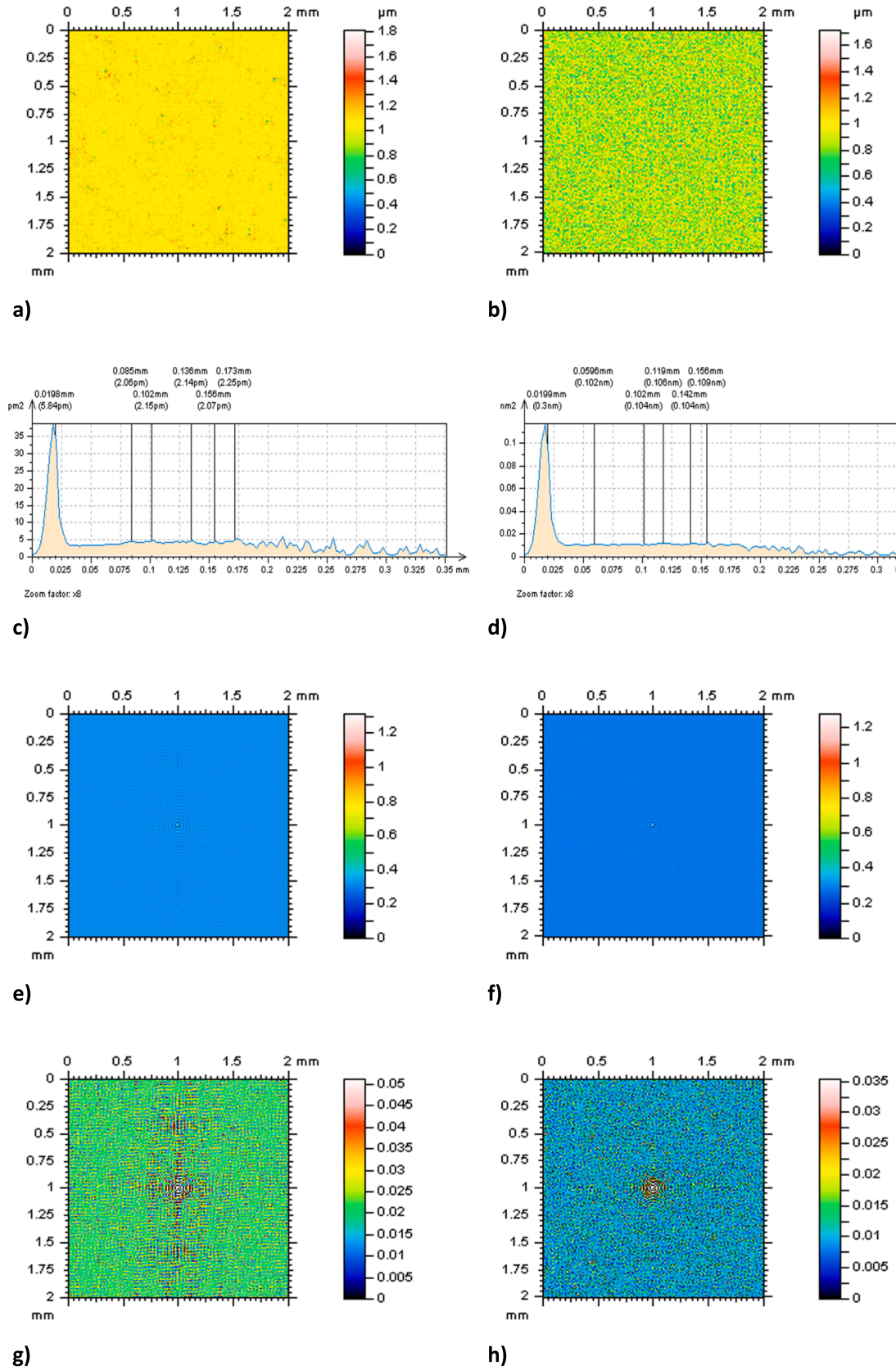

Fig. 8. Contour map plots (a,b) of NS obtained by FFTF (cut-off = 0.20 mm), their PSDs (c,d), ACFs (e,f) and thresholded (0.5 % – 99.5 %) ACFs (g,h), received from raw measured data (left column) and with generated high-frequency noise (right column).

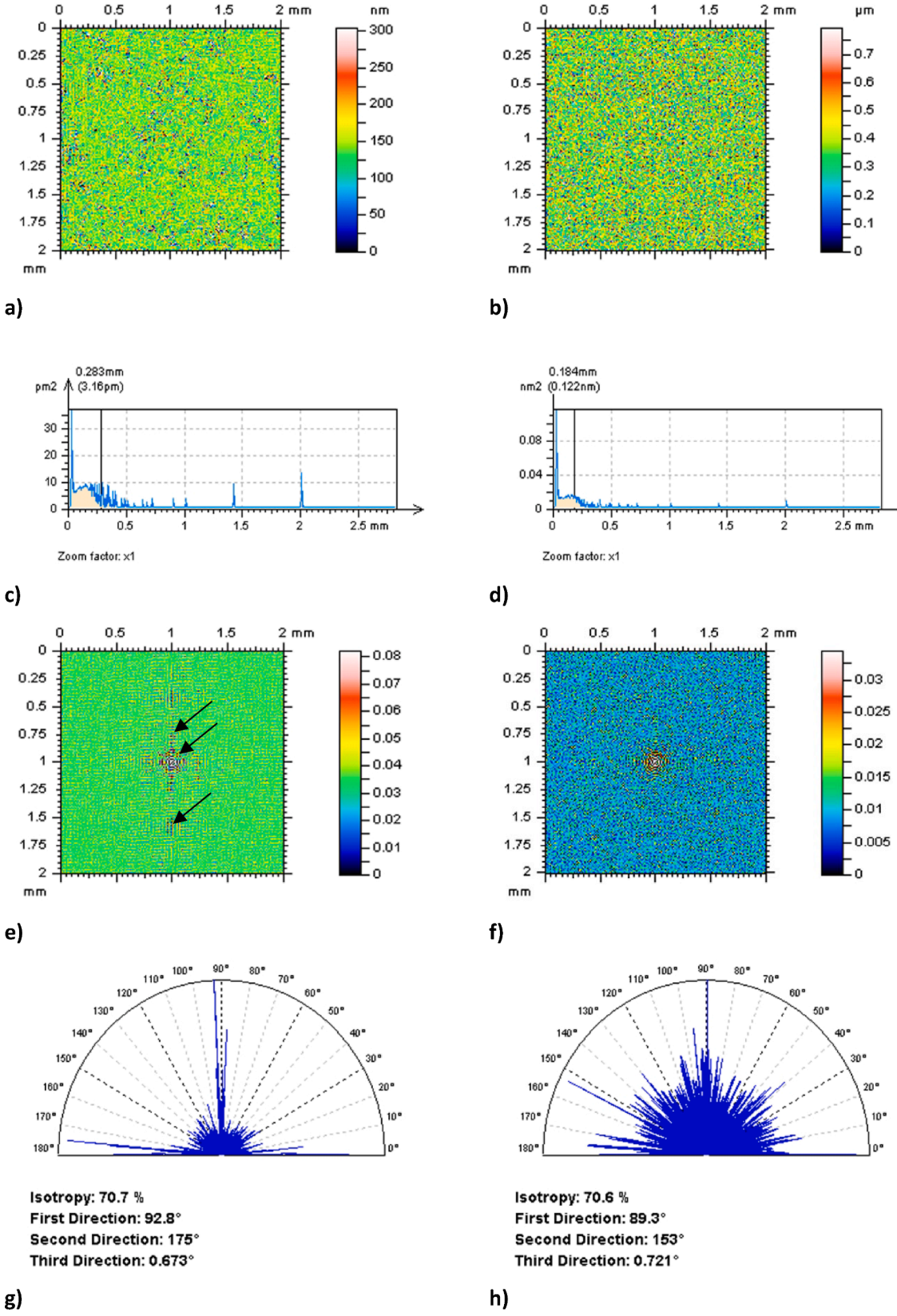

Fig. 9. Contour map plots (a,b) of thresholded NS received by FFTF (cut-off = 0.20 mm), their PSDs (c,d), thresholded (0.5 % – 99.5 %) ACFs (e,f) and TD graphs of the thresholded ACFs received from raw measured data (left column) and with generated high-frequency errors (right column).

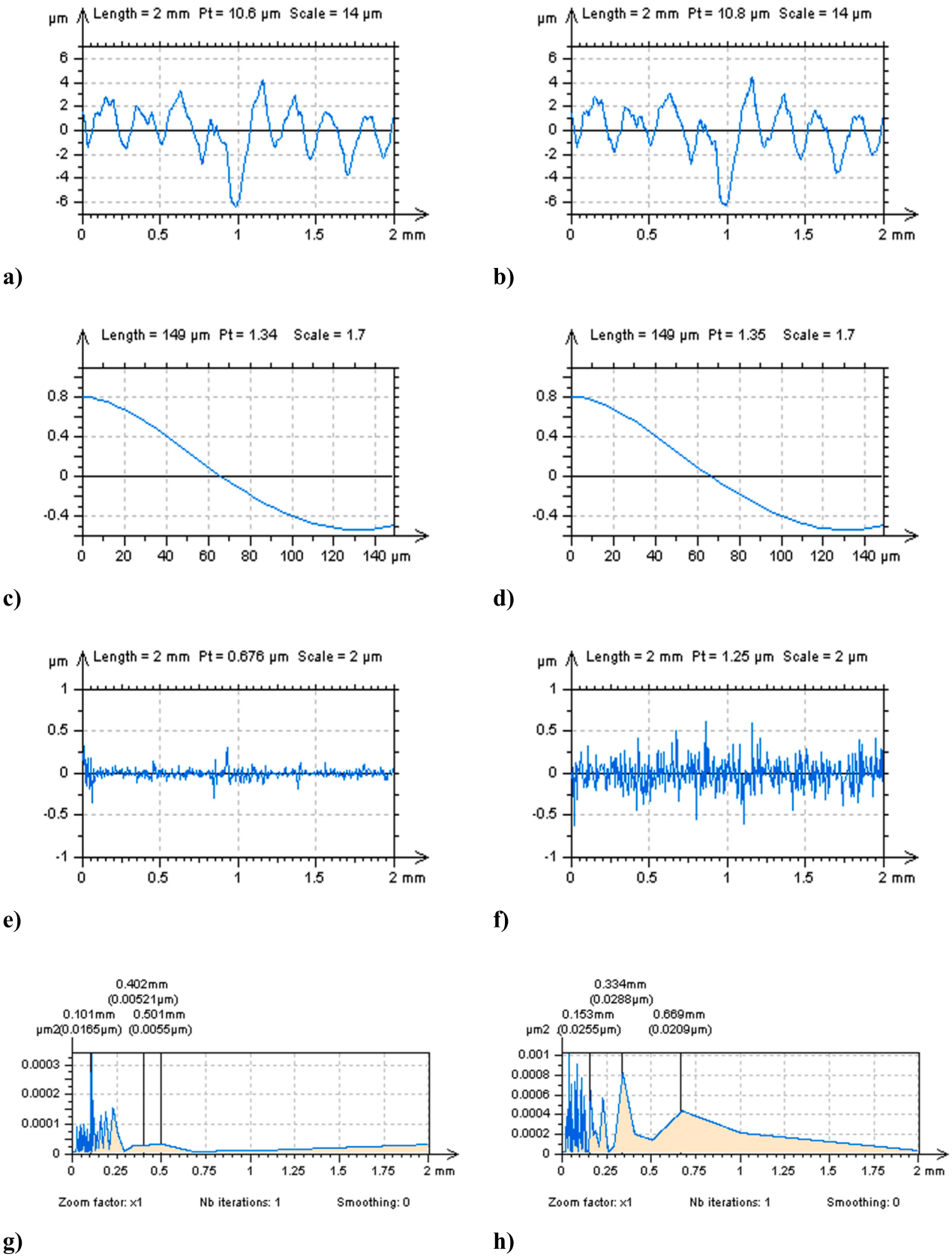

Fig. 10. Profiles after HFN removal (a,b) and their ACFs (c,d), removed HFN (e,f) and their PSDs (g,h), received by application of the FFTF (cut-off = 0.20 mm) method for raw measured data (left column) and with generated high-frequency errors (right column).

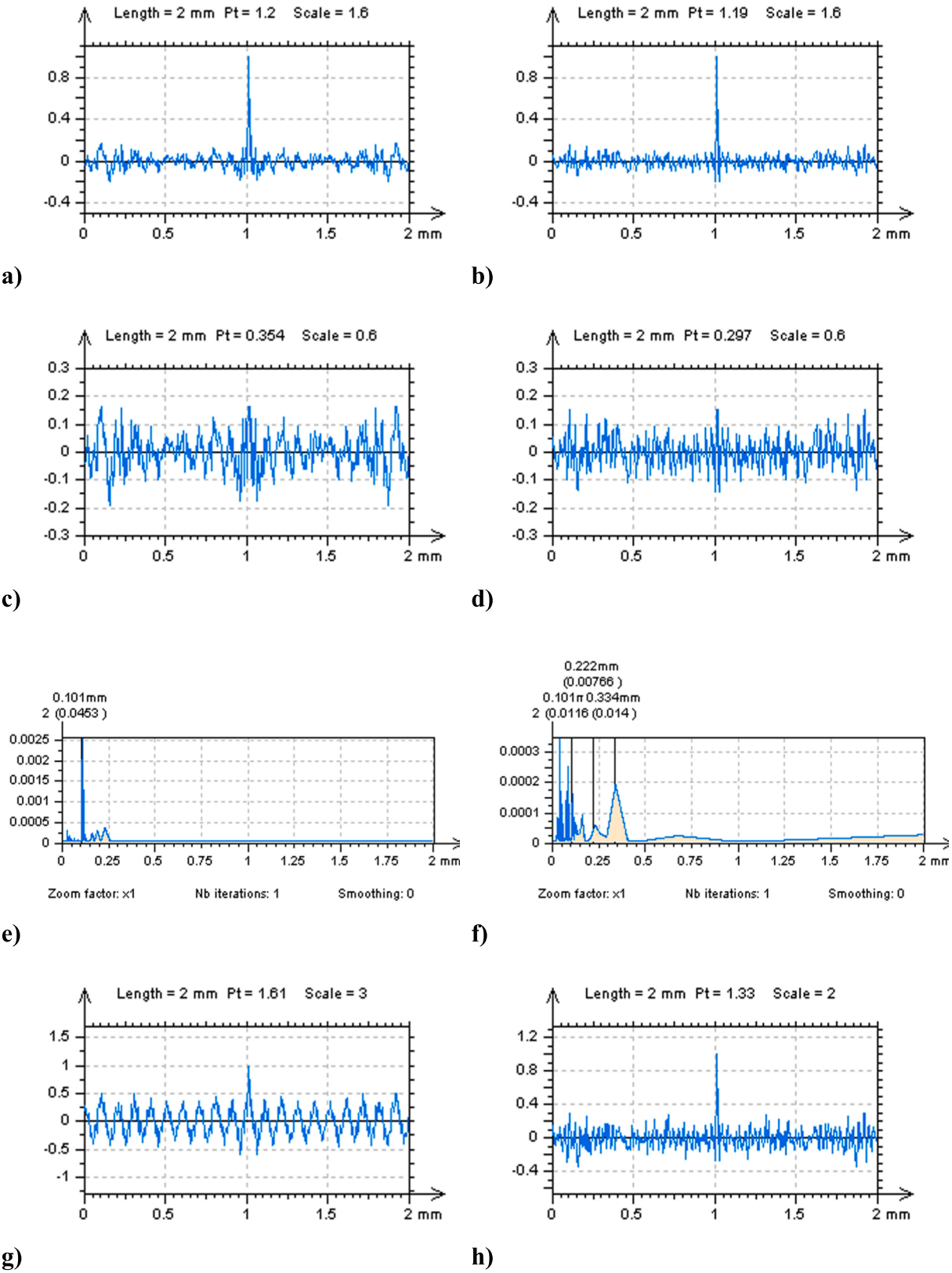

Fig. 11. Received from NSs profiles: ACFs (a,b), their thresholded ACFs (c,d), the PSDs calculated for the thresholded ACFs (e,f) and the ACFs calculated for the thresholded ACFs (g,h); the NS received by FFTF (cut-off = 0.20 mm) filtering of the raw measured data (left column) and filtering the data with generated high-frequency noise (right column).

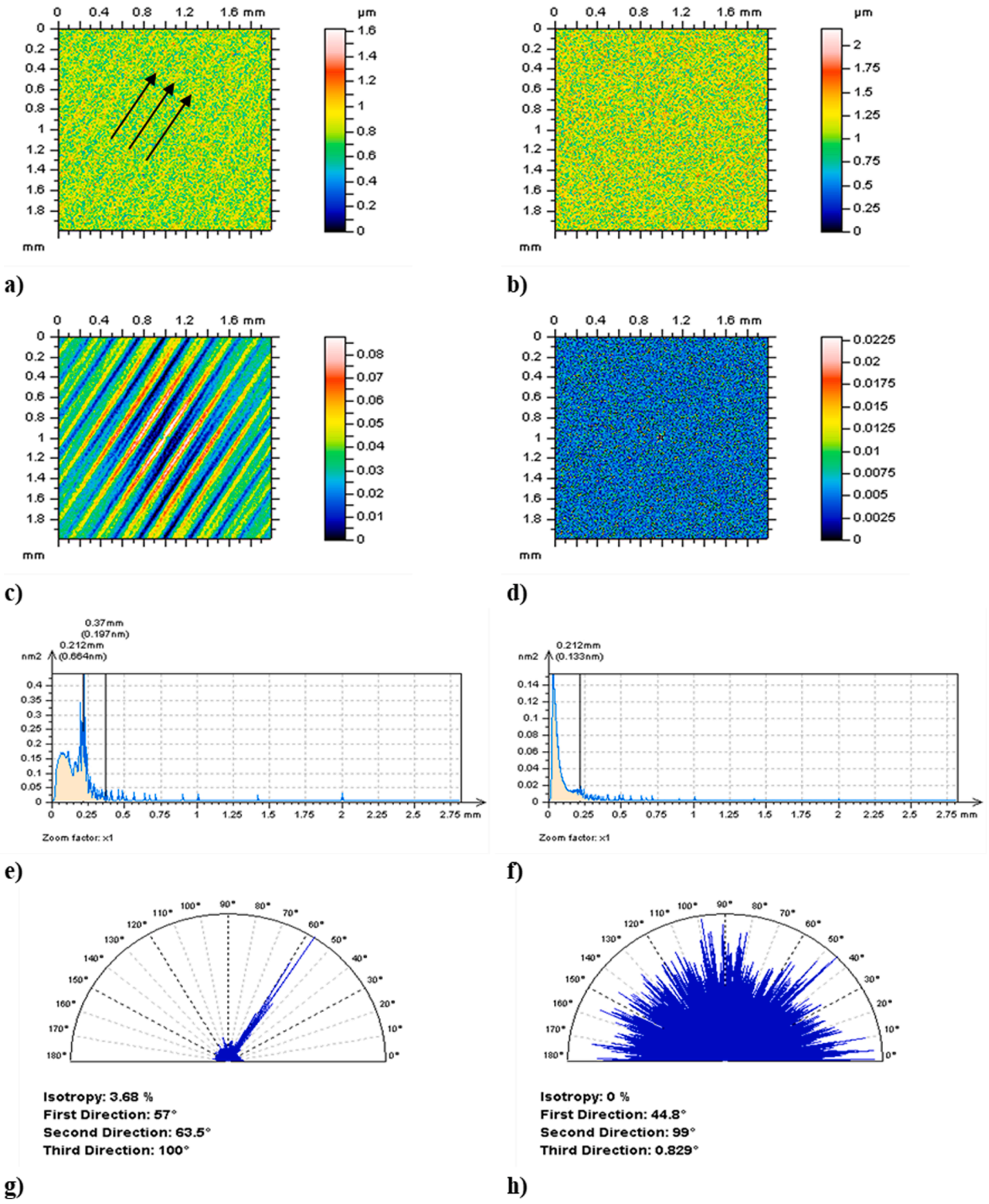

Fig. 12. Contour map plots of NSs (a,b), their thresholded ACFs (c,d), PSDs (e,f) and TD graphs (g,h), received after an HFN removal by application of GRF (a,c,e,g), and SF (b,d,f,h), cut-off = 0.20 mm.

noise data. Further improvement is suggested by using thresholding of the ACF. The thresholded ACFs (e) and their PSDs (f) can determine the dominant frequency. According to the PSD analysis, the dominant frequency for the NS profile obtained after the application of FFTF with a cut-off equal to 0.10 mm and 0.30 mm is equal to 0.25 mm. However, when the 0.20 mm bandwidth was used, the dominant frequency was located in the high-frequency domain. The dominant frequencies can be roughly designated on both the NS profile data (indicated in Fig. 14e) and the PSDs (marked in Fig. 14f). Based on these findings, a cut-off equal to 0.20 mm seems to generate the smallest errors, resulting in non-noise features that are located closest to the high-frequency domains.

The preference for the cut-off value can be simplified with the thresholding improvement. Fig. 15 displays the contour map plots of raw measured data along with their thresholded parts (a,b), which enhances the visibility of eye-view detection of non-noise data in the NSs.

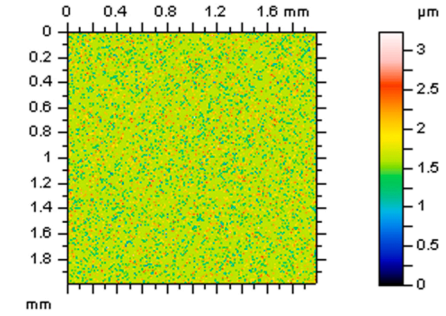

a)

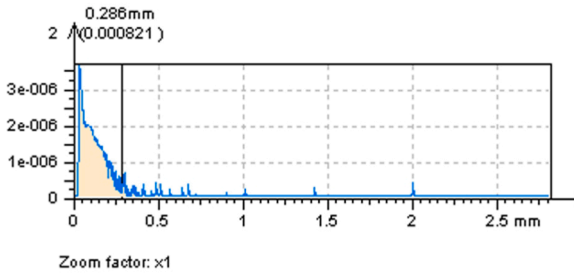

b)

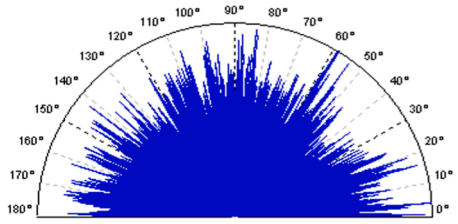

Isotropy: 70.7 %
First Direction: 58.3°
Second Direction: 4.23°
Third Direction: 83.5°

c)

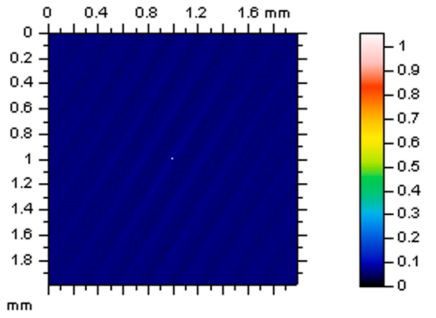

d)

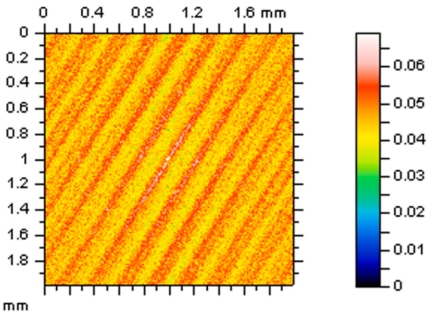

e)

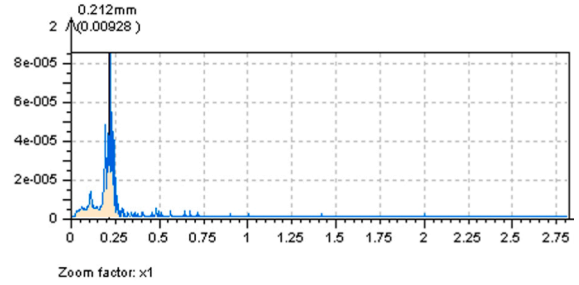

f)

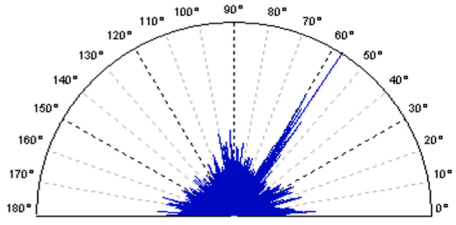

Isotropy: 3.29 %
First Direction: 57°
Second Direction: 92.2°
Third Direction: 100°

g)

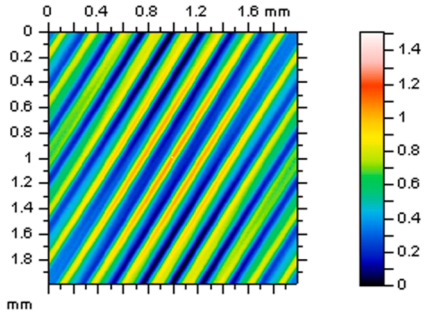

h)

Fig. 13. Contour map plot of NS (a), its PSD (b), TD (c), ACF (d) and the thresholded ACF (e) with its PSD (f), TD (g) and D-ACF (h), received after an HFN suppression by usage the MDF technique, cut-off = 0.20 mm.

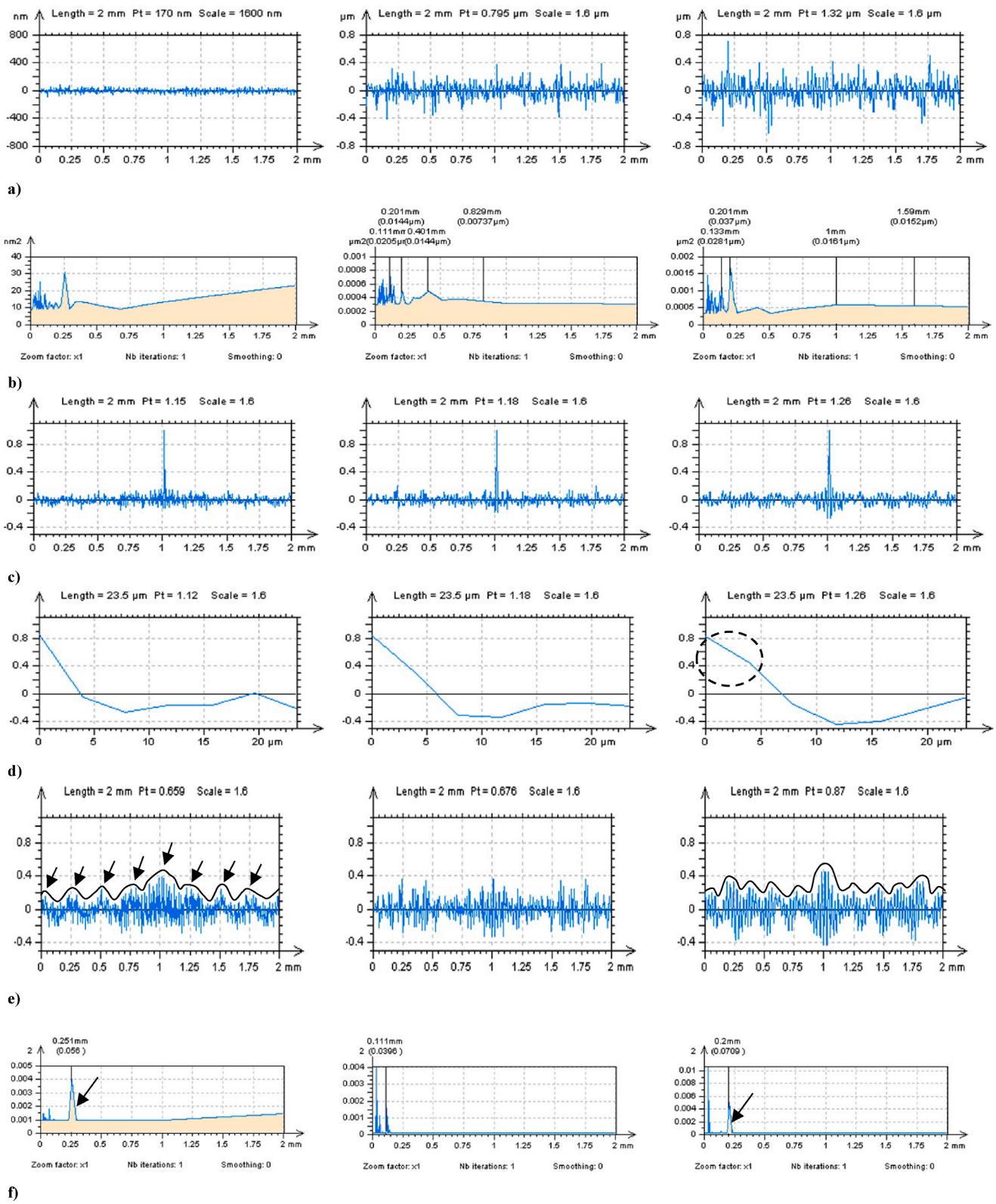

Fig. 14. Profiles extracted from NS (a), their PSDs (b), ACFs (c), enlarged (0.025 mm) ACFs (d), thresholded ACFs (e) and their PSDs (f), received after an HFN reduction by FFTF with cut-off equal to 0.10 mm (left column), 0.020 mm (middle) and 0.030 mm (right column).

The non-noise components are fully visible on the PSD graphs (c,d) and the differences are obvious. However, the results are not supported by the TD graphs (e,f), where the differences are small or negligible. Nevertheless, some responses can be acquired from the analysis of the shape of ACF (g,h).

From the application of the ACF-shape method, especially particularly when the central part is considered, it was found that ACF value increases more rapidly when the RGRF is used against FFTF. In the last 10 µm (first from the left), the value of ACF increased around 0.9 and 0.7 for the RGRF and FFTF methods, respectively. In this study, the shape of

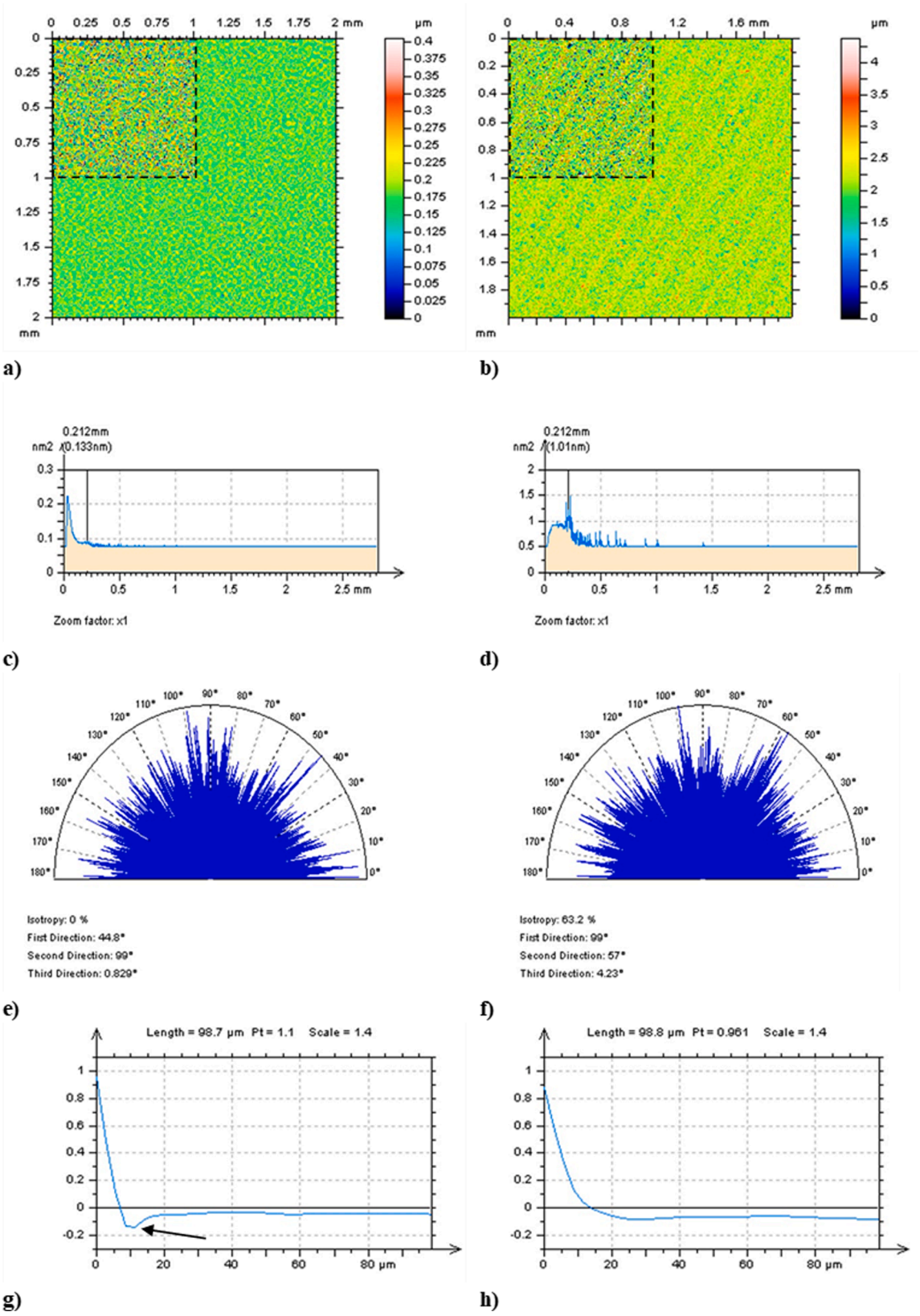

Fig. 15. Contour map plots of NSs (a,b), their PSDs (c,d), TD graphs (e,f) and centre-part of the ACFs (g,h), received after RGRF (left column) and FFTF (right column) filtering with cut-off = 0.010 mm, the dashed line indicates the areas of the NSs thresholding.

ACF can define if the analysed data is on the required frequency. Consequently, reducing the errors in the selection of both filter and its bandwidth (cut-off) for the definition of high-frequency measurement errors depends on a comprehensive analysis of many functions, such as PSD, TD, and ACF. The properties of ACF, in particular, can be extremely valuable in defining measurement noise, especially in the high-frequency domain. Detailed characterisation of the ACF function can improve studies of the surface with a specified direction, such as turned composites.

From a comprehensive analysis of the ACF and PSD functions, it was determined that the most significant contribution of high-frequency components resides within the noisy data (NS), evidenced by the most substantial increase in the centre of the ACF. In practice, when defining the best filtering solution for the reduction of high-frequency noise, the most pronounced amplification near the maximum value (equal to 1) should be identified. Upon evaluating the results obtained from generally available filters in the commercial software, the most promising outcomes were obtained after the implementation of a robust filter (RGRF) with a cut-off equal to 0.010 mm (see Fig. 15g and 15 h). According to the PSD characterisation, the high frequency was dominant after usage of the RGRF method (see Fig. 15c and 15d).

Analysis the high-frequency region [33] of the PSD through refinement of the ACF shape method can effectively determine if selected types of errors are present in the raw measured data. Furthermore, errors caused by false estimation of the noise-removal procedure can be reduced by a comprehensive analysis of both functions. The stability of the procedure for the reduction of selected types of measurement noise (e.g. this in the high-frequency domain) can be enhanced by multithread studies, encompassing the analysis of the high-frequency region of PSD function and the ACF shape, especially in the central region.

The comparison of filtering results between FFTF at 0.020 mm and RGRF at 0.010 mm can lead to relevant outcomes. In both cases, the ACF exhibited the most substantial growth, and the dominant frequency within the PSD was located in the high-frequency domain. However, the increase in ACF for noisy data filtered by FFTF was less pronounced than that observed after the RGRF application. This clearly underscores the importance of analyzing the shape of the autocorrelation function.

It was also found that the presence of high-frequency noise can significantly affect specific surface roughness parameters. According to ISO 25178 standard, the hybrid parameters, including the developed interfacial area ratio Sdr and the root mean square gradient Sdq which represents the Root Mean Square (RMS) surface slope comprising the surface evaluated over all directions, demonstrated the highest sensitivity to the existence of high-frequency noise. In certain instances, these parameters increased by more than 100 % [77]. However, the relative increase of the Sdr parameter was much greater than that of the Sdq, which was consistent with previous studies that hybrid parameters are very sensitive to the occurrence of high-frequency noise [78].

The proposed procedure can be crucial in reducing the errors associated with the calculation of the noise-sensitive ISO 25178 roughness parameters. This includes some hybrid parameters, such as developed interfacial area ratio Sdr and root mean square gradient Sdq, as well as some feature parameters, such as peak density Spd and peak curvature Spc. Among the spatial parameters, the autocorrelation length Sal and texture-aspect ratio Str emerged as the most consistent parameters, aligning with findings from prior research [79].

In essence, appropriately defining the noisy data (referred to as the noise surface, NS) and enhancing it with essential attributes via a comprehensive analysis of the autocorrelation function, namely in terms of its shape, can be crucial in the reduction of errors associated with the evaluation of noise-sensitive ISO 25178 roughness parameters.

4. Conclusions

Based on all studies presented in the previous sections, the following conclusions can be drawn:

1. It was found that errors caused by false raw measured data processing can cause a serious inaccuracy in surface roughness analysis. Even when a precise measuring technique (device) is applied, received data can be processed erroneously. Accordingly, relying solely on highly accurate measuring instruments may not guarantee accurate results if proper data processing techniques are not implemented.
2. Common methods used in surface roughness analysis, such as spectral characterisation (power spectral density), correlation approach (autocorrelation function), and direction of surface texture (texture direction parameter and graph), can be especially helpful in the detection and reduction of selected (in defined frequencies) measurement errors.
3. Analysing the properties of the autocorrelation function, especially its shape, can be beneficial in suppressing high-frequency measurement noise. In some cases, the autocorrelation function can be more effective than other approaches available in commercial software, like power spectral density. However, it is suggested to use more than one function in the characterisation of surface properties. Moreover, it was found that imperfection in the processes of definition and removal of high-frequency measurement errors when a power spectral density function is applied can be reduced when comprehensive studies of the autocorrelation function are conducted.
4. Advanced studies of the shape of the autocorrelation function can be supported by the thresholding technique. This method can be applied to both raw measured data and autocorrelation functions. In both cases, the accuracy of error reduction can be significantly improved.
5. The selection of the cut-off value in the process of high-frequency measurement error reduction must be supported by the characterisation of the data removed, defined as noisy data or noise surface. Required properties of the noise surface can be validated more precisely when the studies are supported by all of the functions appropriately. It was found that noise surface removing the high-frequency measurement errors should consist of only the frequencies of the errors domain.
6. Based on the presented findings, a cut-off equal to 0.010 mm seems to generate the smallest errors in noise-sensitive parameters, resulting in non-noise features that are located closest to the high-frequency domains and that are characterised by the power spectral (PSD) analysis. Moreover, employing the method based on the shape of the autocorrelation function, especially when focusing on the central portion, reveals that the value of the autocorrelation function experiences a more rapid escalation with the utilization of the robust Gaussian filter as compared to the fast Fourier transform and other investigated methods.
7. For the analysis of each type of surface topography, the areal characteristics must be sustained with the profile. It is suggested to use both types of surface roughness studies, including the application of presented functions, simultaneously. In some cases, the areal characterisation of measurement errors did not allow for the definition of the presence of noise appropriately. In such cases, it is suggested to conduct studies on selected profiles with an appropriate extraction process direction.
8. When considering the areal autocorrelation function, some improvements in the detection of high-frequency errors are received when a centre-part (middle) profile is extracted. The process of extraction of the centre profile of the areal autocorrelation function calculated for surface data can be improved with the characterisation of the shape of the function. In this case, the precision in high-frequency noise detection is improved significantly.
9. Finally, all of the commonly used, available in commercial software, filters, can be applied for reducing the influence of high-frequency measurement noise by supporting them with the autocorrelation function characterisation. However, the reduction of errors in data

filtering requires an appropriate procedure, as proposed in this paper.

CRediT authorship contribution statement

Przemysław Podulka: Conceptualization, Methodology, Software, Formal analysis, Investigation, Writing – original draft, Visualization. **Wojciech Macek:** Conceptualization, Methodology, Software, Formal analysis, Investigation, Writing – original draft, Visualization. **Beata Zima:** Software, Validation, Writing – review & editing. **Grzegorz Lesiuk:** Software, Validation, Supervision. **Ricardo Branco:** Methodology, Validation, Writing – original draft, Writing – review & editing. **Grzegorz Królczyk:** Writing – review & editing, Supervision.

Declaration of Competing Interest

The authors declare that they have no known competing financial interests or personal relationships that could have appeared to influence the work reported in this paper.

Data availability

Data will be made available on request.

References

[1] A. Rosenkranz, M. Marian, Combining surface textures and MXene coatings—towards enhanced wear-resistance and durability, Surface Topography: Metrology and Properties 10 (2022) 033001, https://doi.org/10.1088/2051-672X/ac7f4a.

[2] T. Trzepieciński, R. Fejkiel, On the influence of deformation of deep drawing quality steel sheet on surface topography and friction, Tribology International 115 (2017) 78–88, https://doi.org/10.1016/j.triboint.2017.05.007.

[3] P. Harlin, P. Carlsson, U. Bexell, M. Olsson, Influence of Surface Roughness of PVD Coatings on Tribological Performance in Sliding Contacts, Surface and Coating Technology 201 (2006) 4253–4259, https://doi.org/10.1016/j.surfcoat.2006.08.103.

[4] Q.-Y. Deng, S.-P. Zhu, X. Niu, G. Lesiuk, W. Macek, Q. Wang, Load path sensitivity and multiaxial fatigue life prediction of metals under non-proportional loadings, International Journal of Fatigue 166 (2023), 107281, https://doi.org/10.1016/j.ijfatigue.2022.107281.

[5] R. Branco, J.D. Costa, L.P. Borrego, F. Berto, S.M.J. Razavi, W. Macek, Comparison of different one-parameter damage laws and local stress-strain approaches in multiaxial fatigue life assessment of notched components, International Journal of Fatigue 151 (2021), 106405, https://doi.org/10.1016/j.ijfatigue.2021.106405.

[6] D. Rozumek, J. Lewandowski, G. Lesiuk, Z. Marciniak, J.A. Correia, W. Macek, The energy approach to fatigue crack growth of S355 steel welded specimens subjected to bending, Theor. Appl. Fract. Mec. 10 (121) (2022), 103470, https://doi.org/10.1016/j.tafmec.2022.103470.

[7] M. Szala, D. Chocyk, A. Skic, M. Kamiński, W. Macek, M. Turek, Effect of Nitrogen Ion Implantation on the Cavitation Erosion Resistance and Cobalt-Based Solid Solution Phase Transformations of HIPed Stellite 6, Materials 14 (2021) 2324, https://doi.org/10.3390/ma14092324.

[8] H.A. Abdel-Aal, Functional surfaces for tribological applications: Inspiration and design, Surface Topography: Metrology and Properties 4 (2016).

[9] P. Podulka, Selection of Methods of Surface Texture Characterisation for Reduction of the Frequency-Based Errors in the Measurement and Data Analysis Processes, Sensors 22 (2022) 791, https://doi.org/10.3390/s22030791.

[10] A. Dzierwa, Influence of surface preparation on surface topography and tribological behaviours, Arch. Civ. Mech. Eng. 17 (2017) 502–510, https://doi.org/10.1016/j.acme.2016.12.004.

[11] De Groot, P.; De Lega, X.C.; Su, R.; Leach, R. Does interferometry work? A critical look at the foundations of interferometric surface topography measurement. In *Proceedings of the SSPIE Optical Engineering + Applications*, San Diego, CA, USA, 11–15 August **2019**.10.1117/12.2526654.

[12] Leach, R. *Optical Measurement of Surface Topography*. Springer: Berlin, Germany, 2011.10.1007/978-3-642-12012-1.

[13] ISO 25178-600; *Geometric Product Specifications (GPS)–Surface texture: Areal – Part 600: Metrological characteristics for areal topography measuring instruments.* International Organization for Standardization, Geneva, Switzerland, **2019**.

[14] H. Muhamedsalih, X. Jiang, F. Gao, Accelerated Surface Measurement Using Wavelength Scanning Interferometer with Compensation of Environmental Noise, Procedia CIRP 10 (2013) 70–76, https://doi.org/10.1016/j.procir.2013.08.014.

[15] M. Vanrusselt, H. Haitjema, R.K. Leach, P. de Groot, International comparison of noise in areal surface topography measurements, Surface Topography: Metrology and Properties 9 (2021), 025015, https://doi.org/10.1088/2051-672X/abfa29.

[16] R.K. Leach, H. Haitjema, Bandwidth characteristics and comparisons of surface texture measuring instruments, Measurement Science and Technology 21 (2010), 032001, https://doi.org/10.1088/0957-0233/21/3/032001.

[17] P. De Groot, J. DiSciacca, Definition and evaluation of topography measurement noise in optical instruments, Optical Engineering 59 (2020), 064110, https://doi.org/10.1117/1.OE.59.6.064110.

[18] P. Podulka, Proposals of Frequency-Based and Direction Methods to Reduce the Influence of Surface Topography Measurement Errors, Coatings 12 (2022) 726, https://doi.org/10.3390/coatings12060726.

[19] P.J. De Groot, The Meaning and Measure of Vertical Resolution in Optical Surface Topography Measurement, Applied Sciences 7 (2017) 54, https://doi.org/10.3390/app7010054.

[20] P. Hreha, A. Radvanska, L. Knapcikova, G.M. Królczyk, S. Legutko, J.B. Królczyk, S. Hloch, P. Monka, Roughness parameters calculation by means of on-line vibration monitoring emerging from AWJ interaction with material, Metrol. Meas. Syst. 22 (2015) 315–326, https://doi.org/10.1515/mms-2015-0024.

[21] C. Gomez, R. Su, P. de Groot, R.K. Leach, Noise Reduction in Coherence Scanning Interferometry for Surface Topography Measurement, Nanomanuf. Metrol. 3 (2020) 68–76, https://doi.org/10.1007/s41871-020-00057-4.

[22] C.L. Giusca, R.K. Leach, F. Helary, T. Gutauskas, L. Nimishakavi, Calibration of the scales of areal surface topography-measuring instruments: Part 1. Measurement noise and residual flatness, Measurement Science and Technology 23 (2012), 035008, https://doi.org/10.1088/0957-0233/23/3/035008.

[23] P. Podulka, Suppression of the High-Frequency Errors in Surface Topography Measurements Based on Comparison of Various Spline Filtering Methods, Materials 14 (2021) 5096, https://doi.org/10.3390/ma14175096.

[24] W. Macek, R. Branco, M. Szala, Z. Marciniak, R. Ulewicz, N. Szczygiol, P. Kardasz, Profile and Areal Surface Parameters for Fatigue Fracture Characterisation, Materials 13 (2020) 3691, https://doi.org/10.3390/ma13173691.

[25] P. Podulka, Improved Procedures for Feature-Based Suppression of Surface Texture High-Frequency Measurement Errors in the Wear Analysis of Cylinder Liner Topographies, Metals 11 (2021) 143, https://doi.org/10.3390/met11010143.

[26] G. Reina, A. Leanza, A. Milella, A. Messina, Mind the ground: A power spectral density-based estimator for all-terrain rovers, Measurement 151 (2020), 107136, https://doi.org/10.1016/j.measurement.2019.107136.

[27] G.M. Królczyk, R.W. Maruda, P. Nieslony, M. Wieczorowski, Surface morphology analysis of Duplex Stainless Steel (DSS) in Clean Production using the Power Spectral Density, Measurement 94 (2016) 464–470, https://doi.org/10.1016/j.measurement.2016.08.023.

[28] J. Kalisz, K. Żak, S. Wojciechowski, M.K. Gupta, G.M. Krolczyk, Technological and tribological aspects of milling-burnishing process of complex surfaces, Tribology International 155 (2021), 106770, https://doi.org/10.1016/j.triboint.2020.106770.

[29] P. Nieslony, P. Cichosz, G.M. Królczyk, S. Legutko, D. Smyczek, M. Kolodziej, Experimental studies of the cutting force and surface morphology of explosively clad Ti–steel plates, Measurement 78 (2016) 129–137, https://doi.org/10.1016/j.measurement.2015.10.005.

[30] R.K. Leach, C. Evans, L. He, A. Davies, A. Duparré, A. Henning, C.W. Jones, D. O'Connor, Open questions in surface topography measurement: A roadmap, Surface Topography: Metrology and Properties 3 (2015), 013001, https://doi.org/10.1088/2051-672X/3/1/013001.

[31] D.J. Whitehouse, Handbook of surface metrology, Institute of Physics, Bristol and Philadelphia, 1994.

[32] J. Michalski, Surface topography of the cylindrical gear tooth flanks after machining, International Journal of Advanced Manufacturing Technology 43 (2009) 513, https://doi.org/10.1007/s00170-008-1737-5.

[33] Q. Li, Y. Deng, J. Li, W. Shi, Roughness characterization and formation mechanism of abrasive air jet micromachining surface studied by power spectral density, Journal of Manufacturing Processes 57 (2020) 737–747, https://doi.org/10.1016/j.jmapro.2020.07.039.

[34] L. Vepsäläinen, P. Pääkkönen, M. Suvanto, T.A. Pakkanen, Frequency analysis of micropillar structured surfaces: A characterization and design tool for surface texturing, Applied Surface Science 263 (2012) 523–531, https://doi.org/10.1016/j.apsusc.2012.09.098.

[35] S. Roy, A. Bhattacharyya, S. Banerjee, Analysis of effect of voltage on surface texture in electrochemical grinding by autocorrelation function, Tribology International 40 (2007) 1387–1393, https://doi.org/10.1016/j.triboint.2007.03.008.

[36] W.X. Wang, J.Y. Li, W.G. Fan, X.Y. Song, L.F. Wang, Characteristic quantitative evaluation and stochastic modeling of surface topography for zirconia alumina abrasive belt, International Journal of Advanced Manufacturing Technology 89 (9–12) (2016) 3059–3069, https://doi.org/10.1007/s00170-016-9242-8.

[37] W. Grzesik, J. Rech, K. Żak, Characterization of surface textures generated on hardened steel parts in high-precision machining operations, International Journal of Advanced Manufacturing Technology 78 (2015) 2049–2056, https://doi.org/10.1007/s00170-015-6800-4.

[38] P. Podulka, Feature-Based Characterisation of Turned Surface Topography with Suppression of High-Frequency Measurement Errors, Sensors 22 (2022) 9622, https://doi.org/10.3390/s22249622.

[39] P. Hreha, A. Radvanská, S. Hloch, W. Peržel, G.M. Królczyk, K. Monková, Determination of vibration frequency depending on abrasive mass flow rate during abrasive water jet cutting, International Journal of Advanced Manufacturing Technology 77 (2015) 763–774, https://doi.org/10.1007/s00170-014-6497-9.

[40] P. Podulka, The Effect of Surface Topography Feature Size Density and Distribution on the Results of a Data Processing and Parameters Calculation with a Comparison

of Regular Methods, Materials 14 (2021) 4077, https://doi.org/10.3390/ma14154077.
[41] J. Raja, B. Muralikrishnan, S. Fu, Recent advances in separation of roughness, waviness and form, Precision Engineering 26 (2002) 222–235, https://doi.org/10.1016/S0141-6359(02)00103-4.
[42] Iso, 25178–2:2021; *Geometrical product specifications (GPS) — Surface texture: Areal — Part 2: Terms*. Definitions and Surface Texture Parameters, International Organization for Standardization, Geneva, Switzerland, 2021.
[43] P. Podulka, Roughness Evaluation of Burnished Topography with a Precise Definition of the S-L Surface, Applied Sciences 12 (2022) 12788, https://doi.org/10.3390/app122412788.
[44] P. Podulka, Resolving Selected Problems in Surface Topography Analysis by Application of the Autocorrelation Function, Coatings 13 (2023) 74, https://doi.org/10.3390/coatings13010074.
[45] R. Teti, Machining of Composite Materials, CIRP Annals 51 (2) (2002) 611–634, https://doi.org/10.1016/S0007-8506(07)61703-X.
[46] Z. Lei, X. Liu, L. Zhao, A novel 3D stitching method for WLI based large range surface topography measurement, Optics Communication 359 (2016) 435–447, https://doi.org/10.1016/j.optcom.2015.09.074.
[47] F. Mattia, J.-C. Souyris, T. Le Toan, D. Casarano, F. Posa, M. Borgeaud, On the surface roughness characterization for SAR data analysis, Int. Geosci. Remote Se. 2 (1997) 898–900, https://doi.org/10.1109/IGARSS.1997.615291.
[48] Y. Oh, Y.C. Kay, Condition for precise measurement of soil surface roughness, IEEE t. Geosci. Remote 36 (1998) 691–695, https://doi.org/10.1109/36.662751.
[49] A.T. Manninen, Multiscale surface roughness description for scattering modelling of bare soil, Physica A: Statistical Mechanics and its Applications 319 (2003) 535–551, https://doi.org/10.1016/S0378-4371(02)01505-4.
[50] L. Zhixiong, C. Nan, U.D. Perdok, W.B. Hoogmoed, Characterisation of Soil Profile Roughness, Biosystems Engineering 91 (3) (2005) 369–377, https://doi.org/10.1016/j.biosystemseng.2005.04.004.
[51] M.W.J. Davidson, T. Le Toan, F. Mattia, G. Satalino, T. Manninen, M. Borgeaud, On the characterization of agricultural soil roughness for radar remote sensing studies, IEEE Transactions on Geoscience and Remote Sensing 38 (2) (2000) 630–640. https://www.doi.org/10.1109/36.841993.
[52] A. Loew, W. Mauser, A semiempirical surface backscattering model for bare soil surfaces based on a generalized power law spectrum approach, IEEE t. Geosci. Remote 44 (4) (2006) 1022–1035, https://doi.org/10.1109/TGRS.2005.862501.
[53] A.H. Shaw, J. Qu, C. Wang, R.D. England, Tribological study of diesel piston skirt coatings in CJ-4 and PC-11 engine oils, Wear 376–377 (2017) 1673–1681, https://doi.org/10.1016/j.wear.2017.01.082.
[54] L. Convert, E. Bourillot, M. François, N. Pocholle, F. Baras, O. Politano, S. Costil, Laser textured titanium surface characterization, Applied Surface Science 586 (2022), 152807, https://doi.org/10.1016/j.apsusc.2022.152807.
[55] T.R. Martha, N. Kerle, C.J. van Westen, V. Jetten, K.V. Kumar, Segment Optimization and Data-Driven Thresholding for Knowledge-Based Landslide Detection by Object-Based Image Analysis, IEEE t. Geosci. Remote 49 (12) (2011) 4928–4943, https://doi.org/10.1109/TGRS.2011.2151866.
[56] P. Podulka, Thresholding Methods for Reduction in Data Processing Errors in the Laser-Textured Surface Topography Measurements, Materials 15 (2022) 5137, https://doi.org/10.3390/ma15155137.
[57] R. Zahid, H.H. Masjuki, M. Varman, R.A. Mufti, M.A. Kalam, M. Gulzar, Effect of Lubricant Formulations on the Tribological Performance of Self-Mated Doped DLC Contacts: a review, Tribology Letters 58 (2015) 32, https://doi.org/10.1007/s11249-015-0506-5.
[58] H. Singh, K.C. Mutyala, H. Mohseni, T.W. Scharf, R.D. Evans, G.L. Doll, Tribological performance and coating characteristics of sputter-deposited Ti-doped MoS2 in rolling and sliding contact, Tribology Transactions 58 (5) (2015) 767–777, https://doi.org/10.1080/10402004.2015.1015758.
[59] B. Li, P. Li, R. Zhou, X.-Q. Feng, K. Zhou, Contact mechanics in tribological and contact damage-related problems: A review, Tribology International 171 (2022), 107534, https://doi.org/10.1016/j.triboint.2022.107534.
[60] Zakharov, O.V.; Ivanova, T.N.; Pugin, K.G. Variable asymmetric morphological profile filter for roughness analysis. 6th Scientific School Dynamics of Complex Networks and their Applications (DCNA), Kaliningrad, Russian Federation, 2022, 312-315.https://www.doi.org/10.1109/DCNA56428.2022.9923149.
[61] Zakharov, O.V.; Yakovishin, A.S.; Zhukov, A.V. Robustness Analysis of Gaussian Filters for Surface Texture of Additive Manufacturing Products. 2022 International Russian Automation Conference (RusAutoCon), Sochi, Russian Federation, 2022, 28-33. https://www.doi.org/10.1109/RusAutoCon54946.2022.9896266.
[62] M. Ramulu, C.W. Wern, J.L. Garbini, Effect of fibre direction on surface roughness measurements of machined graphite/epoxy composite, Composites Manufacturing 4 (1) (1993) 39–51, https://doi.org/10.1016/0956-7143(93)90015-Z.
[63] K. Peta, M. Mendak, T. Bartkowiak, Discharge Energy as a Key Contributing Factor Determining Microgeometry of Aluminum Samples Created by Electrical Discharge Machining, Crystals 11 (2021) 1371, https://doi.org/10.3390/cryst11111371.
[64] S.G. Croll, Surface roughness profile and its effect on coating adhesion and corrosion protection: A review, Progress in Organic Coatings 148 (2020), 105847, https://doi.org/10.1016/j.porgcoat.2020.105847.
[65] I.A. El-Sonbaty, U.A. Khashaba, A.I. Selmy, A.I. Ali, Prediction of surface roughness profiles for milled surfaces using an artificial neural network and fractal geometry approach, J. Mater. Proces. Tech. 200 (1–3) (2008) 271–278, https://doi.org/10.1016/j.jmatprotec.2007.09.006.
[66] K.J. Kubiak, M.C.T. Wilson, T.G. Mathia, P.h. Carval, Wettability versus roughness of engineering surfaces, Wear 271 (3–4) (2011) 523–528, https://doi.org/10.1016/j.wear.2010.03.029.
[67] C. Yang, U. Tartaglino, B.N.J. Persson, Influence of Surface Roughness on Superhydrophobicity, Physical Review Letters 97 (2006).
[68] B. Hendarto, E. Shayan, B. Ozarska, R. Carr, Analysis of roughness of a sanded wood surface, International Journal of Advanced Manufacturing Technology 28 (2006) 775–780, https://doi.org/10.1007/s00170-004-2414-y.
[69] S. Carmignato, V. Aloisi, F. Medeossi, F. Zanini, E. Savio, Influence of surface roughness on computed tomography dimensional measurements, CIRP Annals 66 (1) (2017) 499–502, https://doi.org/10.1016/j.cirp.2017.04.067.
[70] M.M. Kanafi, A.J. Tuononen, Top topography surface roughness power spectrum for pavement friction evaluation, Tribology International 107 (2017) 240–249, https://doi.org/10.1016/j.triboint.2016.11.038.
[71] V. Ostasevicius, R. Gaidys, J. Rimkeviciene, R. Dauksevicius, An approach based on tool mode control for surface roughness reduction in high-frequency vibration cutting, Journal of Sound and Vibration 329 (23) (2010) 4866–4879, https://doi.org/10.1016/j.jsv.2010.05.028.
[72] S. Chen, R. Feng, C. Zhang, Y. Zhang, Surface roughness measurement method based on multi-parameter modeling learning, Measurement 129 (2018) 664–676, https://doi.org/10.1016/j.measurement.2018.07.071.
[73] C.-C. Kuo, P.-J. Huang, Repeatability and reproducibility study of thin film optical measurement system, Optik 124 (18) (2013) 3489–3493, https://doi.org/10.1016/j.ijleo.2012.10.015.
[74] W. Grabon, P. Pawlus, L. Galda, A. Dzierwa, P. Podulka, Problems of surface topography with oil pockets analysis, Journal of Physics Conference Series 311 (2011), 012023, https://doi.org/10.1088/1742-6596/311/1/012023.
[75] *ISO 25178-3:2012*; Geometrical product specifications (GPS) – Surface texture: Areal – Part 3: Specification operators. International Organization for Standardization: Geneva, Switzerland, 2012.
[76] Z. Li, S. Gröger, Investigation of noise in surface topography measurement using structured illumination microscopy, Metrol. Meas. Syst. 28 (2021) 4, https://doi.org/10.24425/mms.2021.137706.
[77] P. Podulka, Reduction of influence of the high-frequency noise on the results of surface topography measurements, Materials 14 (2021) 333, https://doi.org/10.3390/ma14020333.
[78] D.J. Whitehouse, Handbook of Surface and Nanometrology, CRC Press, Taylor & Francis Group, Boca Raton, 2011.
[79] P. Pawlus, R. Reizer, M. Wieczorowski, G.M. Krolczyk, Study of surface texture measurement errors, Measurement 210 (2023), 112568, https://doi.org/10.1016/j.measurement.2023.112568.